ANNUAL REVIEWS

*Annual Review of Fluid Mechanics*

# Acoustic Tweezers for Particle and Fluid Micromanipulation

M. Baudoin[1] and J.-L. Thomas[2]

[1]Institut d'Electronique de Microélectronique et de Nanotechnologie (IEMN), CNRS UMR 8520, Université de Lille, Ecole Centrale de Lille, Université Polytechnique Hauts-de-France, and Institut Supérieur de l'Electronique et du Numérique (ISEN), 59000 Lille, France; email: michael.baudoin@univ-lille.fr

[2]Institut des NanoSciences de Paris (INSP), CNRS UMR 7588, Sorbonne Université, 75005 Paris, France; email: jean-louis.thomas@upmc.fr

Annu. Rev. Fluid Mech. 2020. 52:205–34

First published as a Review in Advance on August 16, 2019

The *Annual Review of Fluid Mechanics* is online at fluid.annualreviews.org

https://doi.org/10.1146/annurev-fluid-010719-060154



## Keywords

tweezers, acoustical vortices, acoustic radiation pressure, acoustic streaming

## Abstract

Acoustic tweezers powerfully enable the contactless collective or selective manipulation of microscopic objects. Trapping is achieved without pretagging, with forces several orders of magnitude larger than optical tweezers at the same input power, limiting spurious heating and enabling damage-free displacement and orientation of biological samples. In addition, the availability of acoustical coherent sources from kilo- to gigahertz frequencies enables the manipulation of a wide spectrum of particle sizes. After an introduction of the key physical concepts behind fluid and particle manipulation with acoustic radiation pressure and acoustic streaming, we highlight the emergence of specific wave fields, called acoustical vortices, as a means to manipulate particles selectively and in three dimensions with one-sided tweezers. These acoustic vortices can also be used to generate hydrodynamic vortices whose topology is controlled by the topology of the wave. We conclude with an outlook on the field's future directions.

## 1. INTRODUCTION

Acoustic tweezers enable the collective and selective manipulation of particles and fluids with the use of two nonlinear effects: acoustic radiation pressure and acoustic streaming. For particle manipulation, these offer complementary advantages compared to their magnetic and optical analogs. Indeed, one of the first recognized issues with optical tweezers was that the tightly focused laser beam heats the sample and may induce photodamage (Ashkin et al. 1986, Svoboda & Block 1994). This limits the use of optical tweezers for manipulating biosamples, especially when substantial forces ($\geq$100 pN) are required. In contrast, magnetic tweezers have a low trap stiffness since the field is rather constant at the particle scale, and most importantly, magnetic tweezers only enable the manipulation of magnetic particles and otherwise require the target particle to be pretagged (Neuman & Nagy 2008). All of these difficulties are overcome with acoustic tweezers: Indeed, both acoustical and optical radiation pressures are proportional to the intensity of the incoming wave divided by the celerity of the wave. Since the speed of acoustic waves in liquids is five orders of magnitude smaller than light speed, much larger forces can be applied in acoustics than in optics at the same wave intensity, therefore limiting deleterious heating (Baresch et al. 2016). Moreover, acoustic tweezers do not require pretagging. Finally, since ultrasonic sources are available from kilohertz to gigahertz frequencies, particles with sizes ranging from hundreds of nanometers to millimeters can be trapped and manipulated with these devices.

These attractive features led to the early development of acoustical traps (King 1934, Sölner & Bondy 1936). The first systems were based on plane standing waves to trap particles at the nodes or antinodes of the wave depending on their acoustic properties. The emergence of miniaturized transducers enabling on-chip particle trapping (Ding et al. 2012, Tran et al. 2012) has led to a renewed interest in the field, with tremendous developments for practical applications in biology (Ozcelik et al. 2018). On the one hand, plane standing wavefields are relevant for when only one particle is present in the system, for the collective manipulation of multiple objects, or for particle sorting. On the other hand, the multiplicity of nodes and antinodes precludes any selectivity, i.e., one particle cannot be moved independently of other neighboring particles. Moreover, for three-dimensional (3D) particle trapping, the use of standing waves requires some transducers (or reflectors) to be positioned on each side of the trapping area.

The development of selective tweezers (with the ability to manipulate particles individually) requires that the acoustic energy be strongly localized in the area of interest. A natural idea is thus to use focused waves, as in optics (Wu 1991). Nevertheless, one persisting difficulty impeding the development of selective acoustic tweezers is that most particles of interest (e.g., elastic particles, cells, microorganisms) are denser and stiffer than the fluid and hence are trapped at pressure nodes of acoustic fields (Gorkov 1962). Thus, they are expelled from the wave focus. Another difficulty is to obtain a 3D trap with one-sided tweezers, i.e., with a transducer located on only one side of the manipulated samples (for obvious practical reasons). The difficulty arises since scattering forces resulting from the interaction of the beam with the particle naturally tend to push the particles in the direction of the wave propagation. Trapping particles in this direction with a limited aperture of the transducer is thus a real challenge.

To solve these issues, Baresch et al. (2013a) first proposed to use some specific wavefields called spherical (or focused) acoustical vortices. These focalized helical waves spin around a phase singularity, wherein the intensity vanishes, leading to a pressure intensity minimum at the focal point surrounded by a bright ring of high intensity, ensuring the existence of an acoustical trap. These waves possess some fascinating properties: They are nondiffracting and carry orbital momentum (Hefner & Marston 1999). Baresch et al. (2016) demonstrated the ability of such wavefields to trap particles in 3D with a one-sided wave synthesis system. More recently, Riaud et al. (2017a) and Baudoin et al. (2019) showed that the relatively complex transducer arrays used

by Baresch et al. (2016) can be replaced by a single interdigitated transducer whose spiraling shape encodes the phase of the field like a hologram, hence enabling the selective manipulation of particles in a standard microscopy environment. These spiraling transducers are cheap, flat, easily integrable, and compatible with disposable substrates, enabling their widespread use by the scientific community. Other ways to synthesize acoustical vortices with a single transducer include acoustic lenses made of metascreen (Li et al. 2015, Jiang et al. 2016) and spiral diffraction gratings (Jiménez et al. 2016, 2018).

Acoustical vortices enable not only particle manipulation but also fluid manipulation with the use of acoustic streaming (Anhäuser et al. 2012, Riaud et al. 2014, Hong et al. 2015). In particular, they enable the synthesis of hydrodynamic vortices whose topology is controlled by the topology of the acoustical vortex and not by the boundary conditions. This might lead to tremendous developments in microfluidics or in the fundamental study of hydrodynamic vortices.

In Section 2, we introduce the fluids mechanical concepts involved in particle and fluid manipulation. Section 3 discusses the classical manipulation of particles with standing wavefields and the numerous applications at microscales. In Section 4, we introduce some specific wavefields called acoustical vortices and show how they can be used for 3D selective particle and fluid manipulation. Finally, we conclude this review with an outlook on the field's future directions.



## 2. NONLINEAR ACOUSTICS FOR FLUID AND PARTICLE MANIPULATION

### 2.1. Nonlinear Average Equations in Acoustics

At first (linear) order, the time-averaged net force exerted on a particle and the time-averaged fluid flow induced by an acoustic field are null. Thus, the manipulation of particles and fluids requires second-order nonlinear effects. One of these effects, called acoustic radiation pressure, is a net force applied at the interface between two media with different acoustic properties. This force enables the manipulation of particles but also the deformation of fluid interfaces. A second effect, called acoustic streaming, is flow produced by the attenuation of an acoustic wave and the resulting transfer of pseudo-momentum from the wave to the fluid. Depending on the origin of the wave attenuation, acoustic streaming is generally divided into bulk acoustic streaming (also called Eckart streaming), due to thermoviscous damping of the wave in the bulk of the propagating fluid, and boundary streaming (also called Rayleigh streaming), due to wave attenuation at the boundaries resulting from the existence of a viscous boundary layer.

In this section, we derive a set of coupled constitutive equations that allow us to compute (*a*) the nonlinear propagation of acoustic waves, (*b*) bulk acoustics streaming, and (*c*) the force applied on a particle (resulting from acoustic radiation pressure and bulk streaming). All of these equations are derived in the limit of low acoustic Mach number, low acoustic Reynolds number, and low hydrodynamic Reynolds number. Since this review focuses on freely propagating waves, boundary streaming is mostly discarded.

**2.1.1. Constitutive equations.** For the sake of simplicity, we consider here the case of liquids. Hence, the starting point of the following derivation is the isentropic (see the sidebar titled Entropy Balance) compressible Navier–Stokes equations, wherein thermal effects are neglected,

$$\text{Mass balance: } \frac{\partial \rho}{\partial t} + \nabla \cdot (\rho \mathbf{v}) = 0, \qquad 1.$$

$$\text{Momentum balance: } \frac{\partial \rho \mathbf{v}}{\partial t} + \nabla \cdot (\rho \mathbf{v} \otimes \mathbf{v}) = -\nabla p + \mu \Delta \mathbf{v} + \left(\frac{\mu}{3} + \xi\right) \nabla \nabla \cdot \mathbf{v}, \qquad 2.$$

## ENTROPY BALANCE

The fact that viscous effects are considered in the momentum balance but not in the equation of entropy might seem contradictory since viscous effects contribute to the increase of entropy. In fact, since viscous damping is weak and the contribution of viscous effects to the increase of entropy is nonlinear, this approximation is consistent up to second order. Readers are referred to Coulouvrat (1992) for a demonstration with asymptotic analysis.



$$\text{Entropy balance: } \mathrm{d}s = 0, \tag{3.}$$

$$\text{Equation of state: } p = p(\rho), \quad \text{with} \quad \left.\frac{\partial p}{\partial \rho}\right|_s = c_0^2 \quad \text{and} \quad \left.\frac{\partial^2 p}{\partial \rho^2}\right|_s = \Gamma, \tag{4.}$$

where $\rho$, $p$, and $\mathbf{v}$ are the density, pressure, and velocity fields, respectively; $\mu$ is the dynamic viscosity; $\xi$ is the bulk viscosity; $c_0$ is the sound speed; $\Gamma$ equals $\frac{Bc_0^2}{A\rho_0}$; and $A = \rho_0 c_0^2$ and $B$ are two classic acoustics coefficients introduced in nonlinear acoustics.

Thermal effects (wave thermal damping and fluid heating) can be neglected in liquids compared to their viscous counterparts (since they are proportional to $\gamma - 1$, where $\gamma$ is the heat capacity ratio, close to 1 in most liquids). The following theory could be nevertheless completed to account for thermal effects.

**2.1.2. Field decomposition.** Following Riaud et al. (2017b), we then introduce a relevant decomposition of each field $f$ into a hydrostatic contribution $f_0$ (in the absence of acoustic excitation), periodic fluctuations corresponding to the acoustic wave perturbation $\tilde{f}$, and time-averaged contributions $\bar{f}$:

$$\rho = \rho_0 + \tilde{\rho} + \bar{\rho}, \tag{5.}$$

$$p = p_0 + \tilde{p} + \bar{p}, \tag{6.}$$

$$\mathbf{v} = \tilde{\mathbf{v}} + \bar{\mathbf{v}}. \tag{7.}$$

This decomposition differs from the classical decomposition into a zero-, first-, and second-order field in that acoustic wave perturbations can also contain nonlinear effects, as we see below. Since the fluid is assumed to be at rest in the absence of acoustic excitation, $\mathbf{v}_0$ equals $\mathbf{0}$. Mathematically, these fields are defined as $\bar{f} = \langle f - f_0 \rangle$, where $\langle \cdot \rangle$ is the time-averaging operator, and $\tilde{f} = f - f_0 - \bar{f}$ (implying $\langle \tilde{f} \rangle = 0$). We also assume $\tilde{f} \ll \bar{f} \ll f_0$.

**2.1.3. Averaged equations and bulk acoustic streaming.** Time averaging of the constitutive Equations 1–4 up to second order gives

$$\frac{\partial \bar{\rho}}{\partial t} + \rho_0 \nabla \cdot (\bar{\mathbf{v}}) + \frac{1}{c_0^2} \nabla \cdot \bar{\mathbf{I}} = 0, \tag{8.}$$

$$\frac{\partial}{\partial t}\left(\rho_0 \bar{\mathbf{v}} + \frac{1}{c_0^2}\bar{\mathbf{I}}\right) + \rho_0 \nabla \cdot \langle \tilde{\mathbf{v}} \otimes \tilde{\mathbf{v}} \rangle = -\nabla \bar{p} + \mu \Delta \bar{\mathbf{v}} + \left(\frac{\mu}{3} + \xi\right) \nabla \nabla \cdot \bar{\mathbf{v}}, \tag{9.}$$

$$\bar{p} = c_0^2 \bar{\rho} + \frac{\Gamma}{2} \langle \tilde{\rho}^2 \rangle, \tag{10.}$$

where $\bar{I} = \langle \tilde{p}\tilde{\mathbf{v}} \rangle$ is the intensity vector, representing the flux of acoustic energy. These equations are the constitutive equations of the average flow $\bar{\mathbf{v}}$ produced by an acoustic wave, which by definition corresponds to acoustic streaming. By neglecting the fourth-order terms, $\nabla \cdot (\bar{\mathbf{v}} \otimes \bar{\mathbf{v}})$, we have neglected nonlinear hydrodynamics terms. These equations are therefore limited to slow streaming and cannot describe turbulent flows.

Away from boundaries (and the viscous boundary layer), these equations can be simplified with weakly restrictive hypotheses: In the mass conservation equation (Equation 8), the divergence of the intensity vector (third term) corresponds to the viscous dissipation of acoustic energy, which remains weak compared to inertial terms in most media at usual frequencies. This is quantified by the so-called acoustic Reynolds number, $Re_{\mathrm{ac}} = \rho c_0^2/\omega\mu(4/3 + \frac{\xi}{\mu})$, which is also the ratio between the acoustic attenuation length, $L_{\mathrm{a}} = \rho c_0^3/\omega^2\mu(4/3 + \frac{\xi}{\mu})$ (the characteristic distance of the wave damping), and the wavelength, $\lambda$. As a consequence, the condition $Re_{\mathrm{ac}} \ll 1$ ensures that the wave is not attenuated over a distance comparable to the wavelength. The reverse situation only happens in very viscous fluids or at frequencies higher than gigahertz in water. If we assume $Re_{\mathrm{ac}} \ll 1$ and consider only the steady average flow (after the transient state), we obtain the classical Stokes equation,

$$\nabla \cdot \bar{\mathbf{v}} = 0, \tag{11.}$$

$$\mu \Delta \bar{\mathbf{v}} - \nabla \bar{p} + \mathcal{F} = \mathbf{0}, \tag{12.}$$

with a forcing term (Nyborg 1953),

$$\mathcal{F} = -\rho_0 \nabla \cdot \langle \tilde{\mathbf{v}} \otimes \tilde{\mathbf{v}} \rangle, \tag{13.}$$

corresponding to the source of acoustic streaming. As expected, this source is a nonlinear average effect resulting from the acoustic field, $\tilde{\mathbf{v}}$. Owing to its simplicity, this expression of the streaming source term has been widely used to compute acoustic steady streaming numerically. Nevertheless, as we see below, this expression should be avoided, as it contains some terms that do not contribute to bulk acoustic streaming but instead to acoustic radiation pressure, and it can lead to large numerical errors in simulations.

**2.1.4. Periodic fluctuations: nonlinear propagation of the wave.** The equations of the periodic fluctuations up to second order can be simply obtained by subtracting the average Equations 8–10 from the constitutive Equations 1–4,

$$\frac{\partial \tilde{\rho}}{\partial t} + \rho_0 \nabla \cdot \tilde{\mathbf{v}} = -\nabla \cdot \langle\!\langle \tilde{\rho}\tilde{\mathbf{v}} \rangle\!\rangle, \tag{14.}$$

$$\rho_0 \frac{\partial \tilde{\mathbf{v}}}{\partial t} + \nabla \tilde{p} - \mu \Delta \tilde{\mathbf{v}} - \mu b \nabla \nabla \cdot \tilde{\mathbf{v}} = \frac{\partial}{\partial t} \langle\!\langle \tilde{\rho}\tilde{\mathbf{v}} \rangle\!\rangle - \rho_0 \nabla \cdot \langle\!\langle \tilde{\mathbf{v}} \otimes \tilde{\mathbf{v}} \rangle\!\rangle, \tag{15.}$$

$$\tilde{p} - c_0^2 \tilde{\rho} = \frac{\Gamma}{2} \langle\!\langle \tilde{\rho}^2 \rangle\!\rangle, \tag{16.}$$

where $b$ equals $1/3 + \xi/\mu$ and the operator $\langle\!\langle \cdot \rangle\!\rangle$ is defined by $\langle\!\langle \tilde{f}\tilde{g} \rangle\!\rangle = \tilde{f}\tilde{g} - \langle \tilde{f}\tilde{g} \rangle$. The left-hand sides of these equations correspond to the linear equations of damped acoustic waves. The right-hand sides represent nonlinear effects affecting the propagation of the acoustic waves. Following Riaud et al. (2017b), these equations can be combined to obtain the celebrated Kuznetsov (1970)

equation describing the nonlinear propagation of acoustic waves,

$$\frac{\partial^2\tilde{\phi}}{\partial t^2} - c_0^2\Delta\tilde{\phi} - \frac{\mu b}{\rho_0}\frac{\partial}{\partial t}\Delta\tilde{\phi} = \frac{\partial}{\partial t}\left[\frac{B}{2Ac_0^2}\langle\!\langle\left(\frac{\partial\tilde{\phi}}{\partial t}\right)^2\rangle\!\rangle + \langle\!\langle\left(\nabla\tilde{\phi}\right)^2\rangle\!\rangle\right], \quad 17.$$

where $\tilde{\phi}$ is the velocity potential ($\tilde{\mathbf{v}} = -\nabla\tilde{\phi}$). In this equation, the first two terms on the left-hand side correspond to the d'Alembert wave equation and the third term accounts for the wave viscous damping, while the terms on the right-hand side correspond to nonlinear effects affecting the wave propagation. Here we assumed that $\tilde{\mathbf{v}}$ equals $-\nabla\tilde{\phi}$ and thus that the fluctuation field is irrotational. This is correct away from viscous boundary layers since acoustic modes are by definition irrotational.

The size of the contribution of the nonlinear terms to the wave propagation can be evaluated by comparing the characteristic length of the wave propagation, $L_c$, to the so-called shock distance, $L_s = c_0^2/\omega\beta U_{ac}$, where $U_{ac}$ is the magnitude of the acoustic velocity perturbation and $\beta = 1 + B/2A$ is the so-called nonlinear parameter. Indeed, nonlinear effects are small but nevertheless cumulative. Thus, they can play a significant role over this characteristic distance. The main effect is the generation of harmonics and the transfer of energy to these harmonics, which can eventually turn a sinusoidal wave into an acoustical shock wave (the origin of the term "shock distance"). In many practical applications, the nonlinear propagation terms can be neglected.

**2.1.5. Simplification of the bulk streaming source term.** Following Lighthill (1978) and Riaud et al. (2017b), the streaming source term $\mathcal{F} = -\rho_0\nabla\cdot\langle\tilde{\mathbf{v}}\otimes\tilde{\mathbf{v}}\rangle$ can be recast into a gradient term, which does not contribute to acoustic streaming but, as we shall see later, only to the acoustic radiation force, and another term, which is the sole source of bulk streaming,

$$\mathcal{F} = -\nabla\bar{\mathcal{L}} + \frac{\omega^2\mu b}{\rho_0 c^4}\bar{\mathbf{I}}, \quad 18.$$

where $\bar{\mathcal{L}} = \bar{\mathcal{K}} - \bar{\mathcal{V}}$ is the average acoustic Lagrangian, $\bar{\mathcal{K}} = 1/2\rho_0\langle\tilde{\mathbf{v}}^2\rangle$ is the average acoustic kinetic energy, and $\bar{\mathcal{V}} = \langle\tilde{p}^2\rangle/(2\rho_0 c_0^2)$ is the average potential energy. The main assumption used to obtain this equation is that the fluctuation field $\tilde{\mathbf{v}}$ is irrotational. Then, if we introduce the dynamic pressure of the streaming flow, $\bar{p}^s = \bar{p} + \bar{\mathcal{L}} = c_0^2\bar{\rho} + \Gamma/2\left\langle\tilde{\rho}^2\right\rangle + \bar{\mathcal{L}}$, then the Stokes equation of the streaming flow (Equation 12) can be rewritten as

$$\mu\Delta\bar{\mathbf{v}} - \nabla\bar{p}^s + \mathcal{F}^{\mathcal{S}} = 0, \quad \text{with} \quad \mathcal{F}^{\mathcal{S}} = \frac{\omega^2\mu b}{\rho_0 c^4}\bar{\mathbf{I}}, \quad 19.$$

where $\mathcal{F}^{\mathcal{S}}$ is the sole source of acoustic streaming. This equation shows that, in a confined cavity, the gradient term plays no role in acoustic streaming. It also shows, as expected, that the streaming source depends on the wave damping ($\propto \omega^2\mu b$) and the average acoustic intensity, $\bar{\mathbf{I}}$.

**2.1.6. Force applied on a particle and acoustic radiation force.** Now that we have obtained equations for the acoustic wave propagation and acoustic streaming, we can derive the average force applied on a particle suspended in the fluid. This force, $\bar{\mathbf{F}}_p$, is simply the time average of the stress exerted on the moving interface $S_p(t)$ of the particle,

$$\bar{\mathbf{F}}_p = \left\langle\iint_{S_p(t)}\sigma\cdot\mathbf{n}_p\,\mathrm{d}S\right\rangle, \quad 20.$$

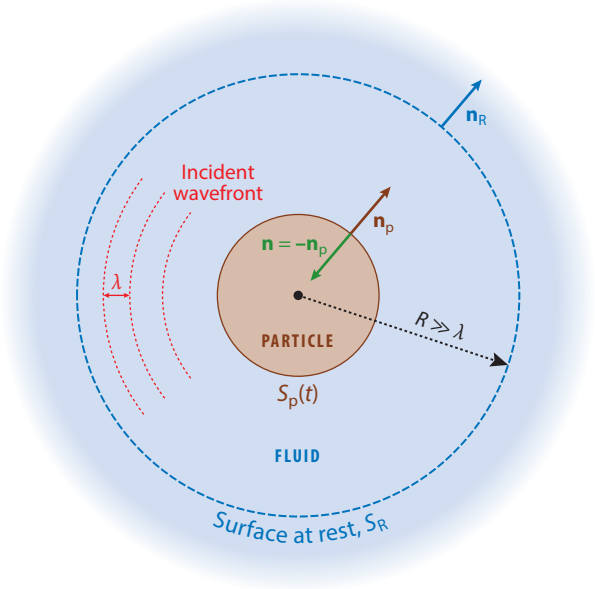


**Figure 1**

Geometry and notations used in the calculation of the force exerted on a particle by an incident acoustic wave. $S_p(t)$ is the vibrating surface of the particle and $R$ is the characteristic radius of a fictitious surface at rest, $S_R$, surrounding the particle.

where $\sigma = -p\mathbf{1} + 2\mu\mathbf{D} + (\xi - 2\mu/3)(\nabla \cdot \mathbf{v})\mathbf{1}$ is the stress tensor and $\mathbf{n}_p$ is the vector normal to the surface of the particle pointing outward (**Figure 1**). The difficulty of performing this integral comes from the vibration of the particle surface induced by the acoustic wave and hence from the fact that it is not fixed. To overcome this difficulty, we can start by introducing the flux of momentum tensor, $\mathcal{B} = \rho\mathbf{v} \otimes \mathbf{v} - \sigma$, and rewrite the momentum balance (Equation 2) as

$$\frac{\partial \rho \mathbf{v}}{\partial t} + \nabla \cdot \mathcal{B} = \mathbf{0}. \qquad 21.$$

Then, we can introduce a closed surface at rest surrounding the particle, $S_R$, and integrate this momentum equation over a volume $V(t)$ bounded on one side by the vibrating surface of the particle, $S_p(t)$, and on the other side by the fixed surface, $S_R$ (see **Figure 1**). The divergence theorem gives

$$\iiint_{V(t)} \frac{\partial \rho \mathbf{v}}{\partial t}\, \mathrm{d}V + \iint_{S_p(t)} \mathcal{B} \cdot \mathbf{n}\, \mathrm{d}S + \iint_{S_R} \mathcal{B} \cdot \mathbf{n}_R\, \mathrm{d}S = \mathbf{0}, \qquad 22.$$

where $\mathbf{n}$ is defined as $-\mathbf{n}_p$ and $\mathbf{n}_R$ is the vector normal to the surface at rest, $S_R$, pointing outward with respect to $V(t)$. The Reynolds transport theorem gives

$$\iiint_{V(t)} \frac{\partial \rho \mathbf{v}}{\partial t}\, \mathrm{d}V = \frac{\partial}{\partial t} \iiint_{V(t)} \rho \mathbf{v}\, \mathrm{d}V - \iint_{S_p(t)} \rho \mathbf{v}\mathbf{v} \cdot \mathbf{n}\, \mathrm{d}S. \qquad 23.$$

Since the first term on the right-hand side vanishes when averaged over time, if we replace the time-averaged Equation 23 into the time-averaged Equation 22, we obtain

$$\bar{\mathbf{F}}_\mathrm{p} = \left\langle \iint_{S_\mathrm{p}(t)} \sigma \cdot \mathbf{n}_\mathrm{p}\, \mathrm{d}S \right\rangle = -\iint_{S_\mathrm{R}} \bar{\mathcal{B}} \cdot \mathbf{n}_\mathrm{R}\, \mathrm{d}S, \tag{24.}$$

with the average momentum flux tensor equal to $\bar{\mathcal{B}} = \rho_0 \langle \tilde{\mathbf{v}} \otimes \tilde{\mathbf{v}} \rangle + (p_0 + \bar{p})\mathbf{1} - 2\mu\bar{\mathbf{D}} - (\xi - 2\mu/3)\nabla \cdot \bar{\mathbf{v}}$ up to second order. Finally considering $\bar{p} = \bar{p}^\mathrm{s} - \bar{\mathcal{L}}$ and $\nabla \cdot \bar{\mathbf{v}} = 0$, we obtain the following final expression of the force applied on a particle,

$$\bar{\mathbf{F}}_\mathrm{p} = \bar{\mathbf{F}}_\mathrm{rad} + \bar{\mathbf{F}}_\mathrm{str}, \tag{25.}$$

$$\text{with } \bar{\mathbf{F}}_\mathrm{rad} = \iint_{S_\mathrm{R}} (-\rho_0 \langle \tilde{\mathbf{v}} \otimes \tilde{\mathbf{v}} \rangle + \bar{\mathcal{L}}) \cdot \mathbf{n}_\mathrm{R}\, \mathrm{d}S, \tag{26.}$$

$$\text{and } \bar{\mathbf{F}}_\mathrm{str} = \iint_{S_\mathrm{R}} (-\bar{p}^\mathrm{s}\mathbf{1} + 2\mu\bar{\mathbf{D}}) \cdot \mathbf{n}_\mathrm{R}\, \mathrm{d}S. \tag{27.}$$

(Since integration is performed here on a closed surface, Equations 26 and 27 are unaffected by any constant $C$. This constant is nevertheless important when Rayleigh radiation pressure is under consideration; readers are referred to Section 2.2.1 for the definition of Rayleigh radiation pressure and Langevin radiation pressure, and to the discussion in Section 2.2.3.) As we see in the next section, the first component of the force $\bar{\mathbf{F}}_\mathrm{rad}$ is the so-called radiation force applied on the particle, while obviously the second component of the force $\bar{\mathbf{F}}_\mathrm{str}$ is simply the force applied on the particle by the average flow, i.e., bulk acoustic streaming.

**2.1.7. Nonlinear acoustics in a nutshell.** As a conclusion to this section, acoustic wave propagation, bulk acoustic streaming, and the force applied on a particle can be summarized by the following set of coupled nonlinear equations,

$$\text{Acoustic wave propagation (linear case): } \frac{\partial^2 \tilde{\phi}}{\partial t^2} - c_0^2 \Delta\tilde{\phi} - \frac{\mu b}{\rho_0}\frac{\partial}{\partial t}\Delta\tilde{\phi} = 0, \tag{28.}$$

$$\text{Bulk acoustic streaming: } \mu\Delta\bar{\mathbf{v}} - \nabla\bar{p}^\mathrm{s} + \mathcal{F}^\mathcal{S} = 0, \text{ with } \mathcal{F}^\mathcal{S} = \frac{\omega^2 \mu b}{\rho_0 c^4}\bar{\mathbf{I}} \text{ and } \bar{\mathbf{I}} = \langle \tilde{p}\tilde{\mathbf{v}} \rangle, \tag{29.}$$

$$\text{Force exerted on a particle: } \bar{\mathbf{F}}_\mathrm{p} = \bar{\mathbf{F}}_\mathrm{rad} + \bar{\mathbf{F}}_\mathrm{str}, \tag{30.}$$

$$\text{Radiation force: } \bar{\mathbf{F}}_\mathrm{rad} = \iint_{S_\mathrm{R}} (-\rho_0 \langle \tilde{\mathbf{v}} \otimes \tilde{\mathbf{v}} \rangle + \bar{\mathcal{L}}) \cdot \mathbf{n}_\mathrm{R}\, \mathrm{d}S, \tag{31.}$$

$$\text{Streaming force: } \bar{\mathbf{F}}_\mathrm{str} = \iint_{S_\mathrm{R}} (-\bar{p}^\mathrm{s}\mathbf{1} + 2\mu\bar{\mathbf{D}}) \cdot \mathbf{n}_\mathrm{R}\, \mathrm{d}S. \tag{32.}$$

## 2.2. Radiation Pressure: A Historical Perspective

The force $\mathbf{F}_\mathrm{p}$ applied by a wave on a particle is at first order an oscillating phenomenon whose temporal average is zero. The existence of a nonzero average force $\bar{\mathbf{F}}_\mathrm{p}$ dates back to Kepler's observation of the orientation of a comet's tail with respect to the light emitted by the sun. The

corpuscular theories of light at that time are probably responsible for the use of the term "radiation pressure" to name the mean force per unit area, $\bar{\mathcal{P}}_{\text{em}}$, due to the pressure in a gas. In this analogy, the radiation pressure of a light wave is always perpendicular to the surface of the illuminated object. Maxwell was the first to propose a coherent theory of this phenomenon and demonstrated that light can instead exert a force in its direction of propagation (Jackson 1962). In this theory, the radiation pressure is given by the average of the electromagnetic stress tensor. A more correct term would therefore be the radiation stress, and this point is responsible for many misunderstandings on this subject. This nonlinear phenomenon proportional to the square of the electromagnetic field has (for a plane wave propagating along the $z$-axis) an amplitude equal to the energy density of the wave, $\bar{\mathcal{P}}_{\text{em}} \cdot \mathbf{z} = \bar{E}_{\text{em}}$. By analogy with point mechanics, the existence of a nonzero mean force leads to the existence of a linear momentum carried by electromagnetic waves. This hypothesis was later confirmed by relativity and led to the equivalence between mass and energy that relates photon momentum and energy.

**2.2.1. Radiation pressure in acoustics.** It was in this historical context, just before the advent of relativity, that Rayleigh proposed and modeled the existence of a radiation pressure for acoustic waves in fluids. He studied the plane wave case and initially obtained an expression identical to optics: The radiation pressure is a second-order phenomenon equal to the time-averaged acoustic energy density, $\bar{E}_{\text{a}}$ (Rayleigh 1902),

$$\bar{\mathcal{P}}_{\text{a}} = \bar{E}_{\text{a}} = \bar{\mathcal{K}} + \bar{\mathcal{V}}. \qquad 33.$$

This naturally led him to postulate the existence of a linear momentum carried by an acoustic wave and to explain the acoustic radiation pressure by an exchange of momentum, similar to optics, following the point of view of Poynting (McIntyre 1981, Post 1960). Nevertheless, for an acoustic wave propagating in a material medium, taking into account the nonlinearity of its state equation, Rayleigh obtained a second expression (Rayleigh 1905, Post 1953),

$$\bar{\mathcal{P}}_{\text{a}} = \beta \bar{E}_{\text{a}}, \qquad 34.$$

with $\beta = 1 + B/(2A)$. This expression, now called the Rayleigh radiation pressure, differentiates the acoustic case from the optical one since the material medium must be taken into account. The proportionality of acoustic radiation pressure and energy density was demonstrated by Altberg (1903). The situation studied by Rayleigh corresponds to a plane wave of infinite lateral extension or a plane mode in a waveguide. This situation is quite far from the practical case where one seeks to manipulate solid or fluid particles completely immersed in a fluid. Langevin was the first to propose a relevant model for this case during a colloquium. His work was nevertheless published only nine years later by Biquard (1932a). Using the Kelvin circulation theorem, Langevin showed that in the stationary regime, the mean pressure difference between two points O and M of a fluid is equal to the difference of acoustic energy density between these two points, $\bar{p}^{\text{L}}_{\text{O}} - \bar{p}^{\text{L}}_{\text{M}} = \bar{E}_{\text{O}} - \bar{E}_{\text{M}}$, where the superscript L stands for Lagrangian coordinates to differentiate from Eulerian coordinates. Selecting for M, a point where the medium is at rest, yields

$$\bar{p}^{\text{L}} = \bar{E}_{\text{a}} + C, \qquad 35.$$

with $C$ a constant. As a consequence, the component related to the nonlinearity of the state equation (see Equation 34) contributes only through a uniform pressure, $C$, which consequently cannot give rise to any overall force for a completely immersed object since it applies on all sides of the object. Thus, Langevin recovered Equation 33, the equivalent of the optical case, known today as the Langevin radiation pressure. The computation in Eulerian coordinates was also made assuming

an irrotational particle velocity and using the unsteady Bernoulli theorem,

$$\bar{p} = \bar{p}^{\mathrm{L}} - 2\bar{K} = -\bar{\mathcal{L}} + C. \qquad 36.$$

This was published in a second article (Biquard 1932b). These two calculations of the average pressure in a fluid in Lagrangian and Eulerian coordinates (Equations 35 and 36) are called the first and second Langevin relations, respectively. This last relation has been revisited by King (1934), Richter (1940), Bopp (1940), and others. We propose here a new version. Indeed, Equation 19 yields $\nabla \bar{p}^{\mathrm{s}} = 0$ for an ideal fluid, so that Equation 36 is recovered from the definition $\bar{p}^{\mathrm{s}} = \bar{p} + \bar{\mathcal{L}}$.

At this point in history, some confusions still remained about the origin and nature of acoustic radiation pressure: First, the average force per unit area exerted by the acoustic wave was considered at that time to be a pressure, i.e., a stress tensor equal to the identity tensor times a scalar. Second, Rayleigh considered the linear momentum carried by an acoustic wave and its transfer to another medium to be responsible for the radiation pressure.

**2.2.2. Radiation stress tensor and acoustic momentum.** This situation was reanalyzed by Brillouin (1925a,b). A good account in English of the content of his papers, published originally in French, can be found in his book (Brillouin 1938).

First, Brillouin challenged the existence of a momentum carried by a longitudinal acoustic wave in a fluid, i.e., he demonstrated that acoustic waves can very well exist without any average momentum (i.e., without any mass flow, since acoustic waves are supported by a medium and the average momentum also corresponds to the average mass flow).

Indeed, the mean momentum in both Eulerian and Lagrangian coordinates is

$$\rho_0 \bar{\mathbf{v}}^{\mathrm{L}} = \langle \rho \mathbf{v}^{\mathrm{E}} \rangle = \langle \tilde{\rho} \tilde{\mathbf{v}} \rangle + \rho_0 \bar{\mathbf{v}}. \qquad 37.$$

Hence, a zero average momentum, i.e., a zero material velocity, $\bar{\mathbf{v}}^{\mathrm{L}} = 0$, does not prevent the existence of an acoustic wave (with density and velocity fields $\tilde{\rho}$ and $\tilde{\mathbf{v}}$, respectively) but instead leads to a nonzero average velocity in Eulerian coordinates, $\bar{\mathbf{v}} = -\langle \tilde{\rho} \tilde{\mathbf{v}} \rangle / \rho_0$. This second-order difference between the particle velocity in Lagrangian and Eulerian coordinates, $\langle \tilde{\rho} \tilde{\mathbf{v}} \rangle / \rho_0 = \bar{\mathbf{v}}^{\mathrm{L}} - \bar{\mathbf{v}}$, is called the Stokes drift. Hence, the acoustic radiation pressure exerted by these waves cannot be explained by an exchange of momentum between the wave and the irradiated object. The quantity $\langle \tilde{\rho} \tilde{\mathbf{v}} \rangle$ is not a true momentum and should instead be called pseudo-momentum or quasi-momentum for quasi-particles like phonons (McIntyre 1981, Peierls 1985, Thomas et al. 2017).

Second, Brillouin stated that the force exerted on the object is the integral of the Cauchy stress on its surface oriented toward the outside (see Equation 20). In the special case of a perfect fluid, the Cauchy stress tensor is the opposite of the pressure times the unit tensor, $-p\mathbf{1}$. The radiation force is thus the following average quantity,

$$\bar{\mathbf{F}}_{\mathrm{p}} = -\left\langle \iint_{S_{\mathrm{p}}(t)} p \mathbf{n}_{\mathrm{p}} \, \mathrm{d}S \right\rangle = -\left\langle \iiint_{V(t)} \nabla p \, \mathrm{d}V \right\rangle, \qquad 38.$$

where we use the divergence theorem to get the second equality. It is important to note that in this expression, the surface $S_{\mathrm{p}}(t)$ of the object driven by the acoustic wave deforms to follow the vibrations of the surrounding medium and thus ensures the continuity of the normal velocity at the interface. Since the surface elements vary in time, the average and integral operators do not commute and $\tilde{p}$ will contribute to the radiation pressure. This definition of the radiation force is difficult to use in practice. An exception is the Bjerknes force on a spherical bubble smaller than the wavelength. At the bubble scale, the pressure gradient is assumed uniform and integration leads to $\bar{\mathbf{F}}_{\mathrm{p}} = -\langle V(t) \nabla \tilde{p} \rangle$, where $V(t)$ is the bubble volume (Bjerknes 1906). This case illustrates

that radiation pressure is a nonlinear phenomenon: The pressure at first order is null on average but cannot be neglected since the surface varies with time.

Third, Brillouin substituted Lagrangian coordinates for Eulerian coordinates in this surface integral. On the one hand, this approach allows one to recover a surface at rest to perform the integral, and on the other hand, the Cauchy stress tensor is transformed into the first Piola–Kirchoff stress tensor. Since the surface is now fixed, the temporal average operation commutes with the integration, and thus integrating the first Piola–Kirchoff average on the rest surface yields the radiation pressure. The first Piola–Kirchoff stress tensor is the momentum flux in the momentum conservation equation in Lagrangian coordinates. The averaged flux of momentum can be finite even if the averaged momentum is null. While this definition is convenient for radiation pressure in solids, an expression in Euler coordinates is preferable in fluids. Hence, Brillouin proposed to use the averaged flux of momentum in Eulerian coordinates on a fixed surface surrounding the object. He noted that going from moving surface elements to fixed ones is exactly compensated for by subtracting the averaged Reynolds stress tensor, so that we have

$$\bar{\mathbf{F}}_\mathrm{p} = -\left\langle \iint_{S_\mathrm{p}(t)} p\mathbf{n}_\mathrm{p}\, \mathrm{d}S \right\rangle = -\left\langle \iint_{S_\mathrm{R}} (p\mathbf{1} + \rho \mathbf{v}\otimes\mathbf{v})\cdot \mathbf{n}_\mathrm{R}\, \mathrm{d}S \right\rangle = -\iint_{S_\mathrm{R}} \bar{\mathcal{B}}\mathbf{n}_\mathrm{R}\, \mathrm{d}S, \qquad 39.$$

where $S_\mathrm{R}$ is a fixed surface surrounding the object (**Figure 1**), and

$$\bar{\mathcal{B}} = (\bar{p} + p_0)\mathbf{1} + \rho_0 \langle \tilde{\mathbf{v}}\otimes\tilde{\mathbf{v}}\rangle \qquad 40.$$

for an inviscid flow. The tensorial nature of radiation pressure has been experimentally verified by Hertz & Mende (1939) and Herrey (1955). This derivation has been generalized by Beissner (1998) in a fluid, and the average fluxes of momentum in Eulerian and Lagrangian coordinates differ only by a curl that does not contribute to the force on a completely immersed object. The direct derivation of Equation 39 from Equation 38, originally introduced by Hasegawa et al. (2000), uses the Reynolds transport theorem and was presented with more generality in Section 2.1.6.

**2.2.3. Integral expression of the force exerted on an immersed particle.** To get an expression valid at second order, one may use the expression of the mean pressure from Equation 36 and substitute it into Equation 40,

$$\bar{\mathcal{B}} = -\bar{\mathcal{L}}\mathbf{1} + (p_0 + C)\mathbf{1} + \rho_0 \langle \tilde{\mathbf{v}}\otimes\tilde{\mathbf{v}}\rangle. \qquad 41.$$

When the object is completely immersed in a perfect fluid (corresponding to Langevin radiation pressure), the integration over a fixed surface surrounding the object cancels the uniform part of the isotropic terms, $(p_0 + C)\mathbf{1}$, and hence the radiation force is obtained by the average of the following tensor (Equation 31) (Brillouin 1936, Bopp 1940, Richter 1940, Borgnis 1953, Post 1953),

$$\bar{\mathcal{B}} = -\bar{\mathcal{L}}\mathbf{1} + \rho_0 \langle \tilde{\mathbf{v}}\otimes\tilde{\mathbf{v}}\rangle. \qquad 42.$$

This tensor is completely determined by the average of a quadratic expression involving $\tilde{p}$ and $\tilde{\mathbf{v}}$; hence, the radiation force on a completely immersed object does not depend on the medium nonlinearity that is contained in the constant $C$. Thus we recover the features of the optical case. This holds as long as the pressure-like term has time to relax and at equilibrium gives a uniform pressure throughout the fluid.

However, when the wave is of infinite aperture or confined in a waveguide (corresponding to Rayleigh radiation pressure), this isotropic uniform term plays a role. Thus the constant $C$ must be

determined from the boundary conditions (Brillouin 1925a). For a plane progressive wave oriented along the $x$-axis impinging upon an absorbing target whose average position is fixed, all fields have a uniform amplitude. Hence we can deduce $\bar{\rho} = 0$ from mass conservation since the whole volume is fixed on average. From Equation 10, we get $\bar{p} = B/A\bar{\mathcal{V}}$, with $B$ and $A$ the two nonlinear coefficients defined below Equation 4. Since for a plane progressive wave we have $\bar{\mathcal{V}} = \bar{\mathcal{K}} = 1/2\bar{E}_a$, we can deduce $\bar{p} = B/(2A)\bar{E}_a$ and $\rho_0\langle\tilde{v}_i\tilde{v}_j\rangle = \bar{E}_a\delta_{11}$. Thus, the radiation stress tensor, Equation 40, reduces to $(p_0 + B/(2A)\bar{E}_a)\delta_{ij} + \bar{E}_a\delta_{11}$. The lateral pressure is $p_0 + B/(2A)\bar{E}_a$, while on the axis of propagation, we get $p_0 + \beta\bar{E}_a$. If the outside pressure is $p_0$, then the excess pressure from the inside is $\beta\bar{E}_a$, i.e., the Rayleigh radiation pressure, Equation 34.

## 2.3. Axial Radiation Force on a Sphere

As underlined above (Equation 42), the radiation pressure tensor depends only on the acoustic field at first order. If we consider a particle irradiated by an acoustic wave, the acoustic field is the sum of the incident and scattered field and thus it is necessary to compute the latter before performing the integration on an arbitrary surface at rest located around the object. These two steps have been achieved by King (1934) for a rigid sphere using Equation 36. Embleton (1954) extended these results to the radiation pressure on a rigid sphere set at the focus of a spherical incident wave. Yosioka & Kawasima (1955) solved the problem of a compressible fluid sphere and then Hasegawa & Yosioka (1969) considered the case of an elastic sphere irradiated by a plane incident wave using Equation 42. Later, the work of Embleton (1954) was generalized to take into account the elasticity of the sphere (Chen & Apfel 1996). An essential step is the computation of the scattered waves and hence the scattering coefficient. For an incident longitudinal plane wave and an elastic sphere, the first derivation was made by Faran (1951). In all of these extensions, axisymmetry was used to considerably simplify the task (Hasegawa et al. 1981). Mathematically, the displacement vector in the elastic spherical particle can be decomposed into a scalar and a vector potential using Helmholtz decomposition. For an incident longitudinal plane wave propagating along the $z$-axis, the axial symmetry allows one to introduce only one component of the vector potential in spherical coordinates, $\mathbf{A} = (0, 0, A(r, \theta))$. The complete problem is thus reduced to two scalars, both solutions of Helmholtz's equation. The two potentials are then written as an infinite sum of spherical modes without azimuthal dependence. The boundary conditions at the sphere surface provide the relation between incident and scattered waves for each spherical mode. Importantly, only the force component in the beam direction can be calculated with this approach. These two limitations (axial symmetry and force component in the beam direction) prevented the use of these models for tweezer investigations and led only to experimental confirmation of theory in academic configurations (Klein 1938, Hasegawa 1977, Rudnick 1977), local acoustic fields measurements complementary of radiation force balance (Rooney 1973), and levitation traps (Sölner & Bondy 1936).

## 2.4. Bulk Acoustic Streaming: A Historical Perspective

As with the history of acoustic radiation pressure, the history of acoustic streaming also starts with the work of Rayleigh (1884). Inspired by Faraday's (1831) and Dvorak's (1874) observations of the flows produced by vibrating plates and Kundt tubes, Rayleigh developed the first theory of the flow induced by an acoustic wave damped by its interactions with the walls of a tube. In this first type of acoustic streaming, the flow results from the wave damping induced by shear stresses in the viscous boundary layer, where the fluid velocity decays to match the velocity of the boundary. This type of streaming is now called boundary streaming or Rayleigh streaming. Later on, with the advent of

piezoelectric generators, many scientists have reported strong flows of air or liquid in the direction of the acoustic wave propagation, termed quartz wind. It was first demonstrated by Eckart (1948) (for liquids) that, in this case, the flow results from the viscous attenuation of the wave in the bulk of the fluid. Indeed, for liquids, the bulk viscous damping is dominant, while in gases, both thermal and viscous damping contribute to acoustic streaming. This second type of acoustic streaming is now called bulk streaming or Eckart streaming. Eckart obtained his results (*a*) by developing the compressible isentropic Navier–Stokes equations into zero-order, first-order (linear), and second-order (nonlinear) contributions; (*b*) by combining the mass and momentum equations at second order; and (*c*) by separating the second-order terms contributing to the nonlinear propagation of the wave from the one contributing to an incompressible flow by taking the divergence and curl of these combined equations, respectively. In this way, Eckart obtained an unsteady diffusion equation for the vorticity (curl of the velocity) at second order, $\mathbf{\Omega}_2 = \nabla \times \mathbf{v}_2$, corresponding to acoustic streaming,

$$\frac{\partial \mathbf{\Omega}_2}{\partial t} - \frac{\mu}{\rho_0} \Delta \mathbf{\Omega}_2 = \frac{b\mu_0}{\rho_0^3} \nabla \rho_1 \times \nabla \frac{\partial \rho_1}{\partial t}, \qquad 43.$$

where $\rho_1$ is the density variation at first order (corresponding to the acoustic wave) and $\mathbf{v}_2$ is the velocity field at second order. He then applied this equation to compute the flow produced in an infinite tube by a weakly attenuated wave of finite aperture propagating along the axis of the tube without lateral interaction with the walls. His theory was verified experimentally soon after by Libermann (1949), who nevertheless noticed some differences with Eckart's theory at large Reynolds number. Indeed, all of these theories based on asymptotic development are only valid for slow streaming flow (low hydrodynamic Reynolds numbers associated with the steady flow). On the one hand, the advantage of Eckart's formulation is that it does not rely on time averaging, and thus these equations allow one to describe unsteady bulk streaming. On the other hand, these equations describe the evolution of the vorticity field, thus it is sometimes difficult to express the boundary conditions in terms of vorticity, and the derivation of the velocity field from the vorticity field requires one to solve another set of differential equations. Nyborg (1953) proposed a formulation corresponding to a Stokes equation with a source term at the origin of the acoustic streaming (corresponding to Equations 11–13). While mathematically sound, his formulation of the source term is to proscribe numerically since it contains some potential terms (see Equation 18) that do not contribute to acoustic streaming but can be several orders of magnitude larger than the actual source term. Thus, small numerical errors in the gradient terms can lead to numerical acoustic streaming resulting from numerical dissipation. Lighthill (1978) identified this gradient term, and later Riaud et al. (2017b) isolated the sole source of bulk acoustic streaming and expressed it as a function of the intensity vector (see Equation 19). These authors also demonstrated that the bulk streaming source term can be spatially filtered, as the small structures of the acoustic field do not contribute to acoustic streaming. Westervelt (1953) extended Eckart's work and reconciliated bulk and boundary streaming in a single formulation. He showed that his formulation allows one to recover these two types of streaming as limit cases.

Since these pioneering works on bulk streaming, many effects have been studied, such as transient streaming (Rudenko 1971), the influence of diffraction by the edges of the beam (Kamakura 1996, Moudjed et al. 2014), the effect of the nonlinear propagation of the wave (Romanenko 1960, Stanikov 1967), weakly nonlinear flows at intermediate Reynolds numbers in the limit of the conservation of the flow symmetry (Gusev & Rudenko 1979), and, more recently, the effect of fluid inhomogeneity (Karlsen et al. 2016). However, despite these efforts, a proper theory of fast acoustic bulk streaming at high Reynolds numbers is still lacking. In this short historical review, we

do not cover the extensive fields of the flow produced by the interaction of a sound wave with a particle or a bubble, nor do we treat the steady streaming produced by incompressible alternative flows (Riley 2001).

## 3. ACOUSTICAL TRAPS AND COLLECTIVE MANIPULATION WITH STANDING WAVES

### 3.1. Historical Development of the Field

While the first theoretical works on radiation pressure were performed in optics, the first effective setups for particle trapping were developed in acoustics. The main reason for this was the availability of a powerful coherent source that appeared later in optics than in acoustics with the development of lasers. Thus, the collective manipulation of particles with standing waves has a long history going back to Chladni figures and Kundt tubes. Chladni figures illustrate that very small particles are driven mostly by acoustic streaming, while the radiation force dominates for larger particles (Hagsäter et al. 2007). The relation between these standing wave acoustical traps and radiation pressure, as modeled by King (1934), was clearly established by Sölner & Bondy (1936). Allen & Rudnick (1947) observed the levitation of different items in standing and progressive waves in air using a very powerful siren operating at 25 kHz. They noted that while relatively large objects could be levitated by a standing wave, the trap was unstable for progressive waves. The levitation of bubbles in liquid columns vibrating at low frequency was also observed and explained by the Bjerknes force (Bucchanan et al. 1962, Baird 1963). Piezoelectric sources working at higher frequencies were used thereafter to excite the resonant mode of a cylindrical cavity and levitate a single bubble at the pressure antinode at low frequencies (Eller 1968, Gould 1968). Thereafter, these levitation traps were used to study the surface tension and phase transition of liquid drops (Apfel 1981). Levitation traps were developed both in liquid and in air. In air, the radiation force in acoustics is strong enough to levitate millimeter beads of iridium, the material with the highest density (Xie & Wei 2002). The observation of agglomeration of red blood cells was related to acoustic standing wavefields, and it was initially used to assess potential detrimental hazards in medical imaging (Baker 1972). When many particles are involved and interact, there are several forces at play and the discrimination can be be rather complex (Coakley et al. 1989). Nevertheless, it was recognized that radiation pressure in standing waves could be used for both the harvesting and manipulation of small particles (Schram 1984, Whitworth et al. 1991) using modulation of either phase or amplitude of the two counter-propagating plane waves.

### 3.2. Radiation Force on Drops and Elastic Spheres in the Long-Wavelength Regime

The most common expression of the radiation force induced by standing waves assumes (*a*) spherical particles and (*b*) excitation in the long-wavelength regime (i.e., when the wavelength is much larger than the size of the particle). For bubbles, the force is described by the Bjerknes formula. Gorkov (1962) developed a model that is used today in most acoustic traps for the case where the contrast of the compressibility and density between the particle and the surrounding fluid is not too high (e.g., elastic particles or drops in a liquid).

Since the sphere radius is very small compared to the wavelength, $k_0 a \ll 1$, the monopole and dipole scattering dominate, and Gorkov (1962) obtained the following simple expression from a

multipole expansion,

$$\bar{\mathbf{F}}_{\mathrm{p}} = -\nabla\left(\alpha_{\mathrm{m}}\bar{\mathcal{V}} - \alpha_{\mathrm{d}}\bar{\mathcal{K}}\right), \qquad 44.$$

$$\text{with } \alpha_{\mathrm{m}} = \frac{4}{3}\pi a^3\left(1 - \frac{K_0}{K_{\mathrm{p}}}\right) \text{ and } \alpha_{\mathrm{d}} = 4\pi a^3\left(\frac{\rho_{\mathrm{p}} - \rho_0}{2\rho_{\mathrm{p}} + \rho_0}\right).$$

In this formula, $K_0 = \rho_0 c_0^2$ and $K_{\mathrm{p}} = \rho_{\mathrm{p}}(c_{\mathrm{l}}^2 - 4/3c_{\mathrm{t}}^2)$ are respectively the bulk elasticity of the fluid and the particle, $c_{\mathrm{l}}$ and $c_{\mathrm{t}}$ are respectively the particle longitudinal and transverse wave speeds, $\rho_0$ and $\rho_{\mathrm{p}}$ are respectively the fluid and particle densities, and $a$ is the radius of the particle. Here, the potential acoustic energy, $\bar{\mathcal{V}}$, and the kinetic acoustic energy, $\bar{\mathcal{K}}$, are computed with the amplitude of the linear incident field at the sphere location. In this expression, the radiation pressure is a potential force that depends on the incident linear fields and the acoustic contrast factor in compressibility and density. This approximation based on a Taylor expansion is valid as long as the kinetic and potential energies are not uniform in any direction. Since this contribution to the radiation force relies on the gradient of the field, it is generally called the gradient force. This is the case encountered in standing waves. On the contrary, this force cancels out for a plane progressive wave, and the Taylor development must be carried out at the next order. This case was also studied by Gorkov (1962), and in this case, the force is no longer a gradient force but instead a scattering force. In a real fluid, viscosity corrections can be important (Settnes & Bruus 2012), and thermal dissipation has also been considered (Karlsen & Bruus 2015).

### 3.3. Particle Micromanipulation with Radiation Force

Today, a very active field of research combines acoustic standing waves with microfluidics. Many promising biological applications have been developed to separate, concentrate, and manipulate particles, particularly biological cells, in a label-free environment and with high throughput. The literature on this topic is quite extensive and outside the scope of this review; interested readers are referred to existing reviews on the subject (Lenshof & Laurell 2010, Ding et al. 2013, Yeo & Friend 2014, Ozcelik et al. 2018). We can nevertheless highlight three interesting recent developments of the field: (*a*) the miniaturization of tweezers to manipulate micron-size particles and in particular biological cells with the use of surface acoustic waves (Ding et al. 2012, Tran et al. 2012); (*b*) the theoretical (Hasegawa 1979, Silva et al. 2019), experimental (Collins et al. 2015, Silva et al. 2019), and numerical (Glynne-Jones et al. 2013, Habibi et al. 2017, Baasch & Dual 2018) study of standing waves traps beyond the long-wavelength regime; and (*c*) the investigation of the torque applied on nonspherical particles trapped at the nodes of standing wavefields (Schwartz et al. 2013). With standing waves, individual particle manipulations are limited by two adverse effects that forbid selectivity. First, standing waves generate trap locations at each node, antinode, or midpoints (in 2D configurations) depending on the acoustic contrasts of density, compressibility, and the size of the particles (see, e.g., Silva et al. 2019), hence preventing the trapping of one particle independently of other neighboring particles (**Figure 2**). Second, the size and stiffness of the trap is determined by the wavelength, and most of these setups are designed in the long-wavelength regime.

## 4. SELECTIVE ACOUSTIC TWEEZERS AND STIRRERS

### 4.1. Spatial Localization of the Acoustic Energy and Acoustical Vortices

The selective manipulation of a particle, i.e., its manipulation independent of other neighboring particles, can only be achieved through spatial localization of the trap (and hence the acoustic

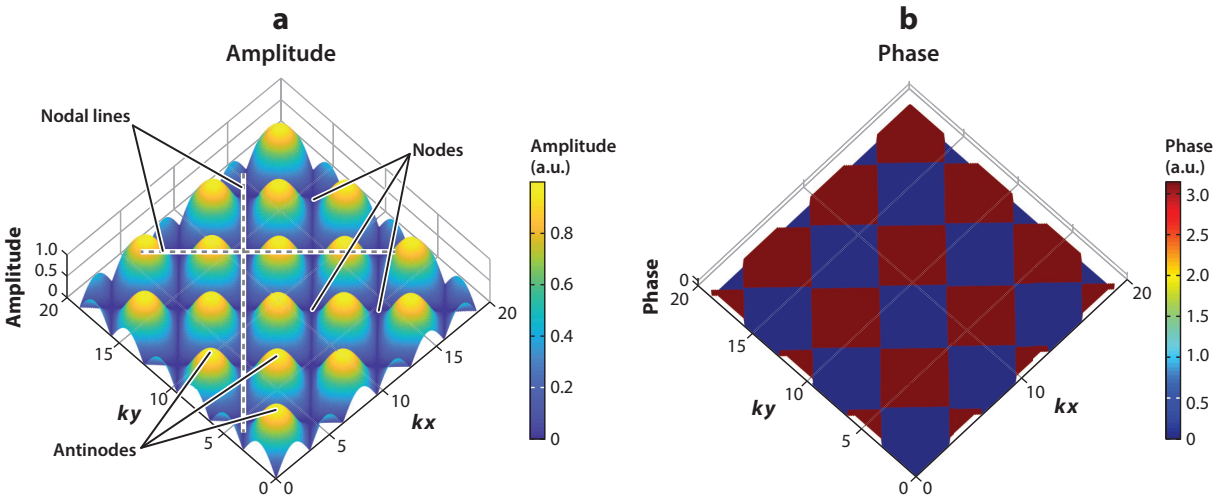


**Figure 2**

Amplitude (*a*) and phase (*b*) of a two-dimensional standing wavefield of the form $\Psi = 1/2[\sin(kx) + \sin(ky)]\exp(i\omega t)$ represented at a given time $t$, where $k = \omega/c_0$ is the wave number, $\omega$ is the angular frequency, and $c_0$ is the sound speed. Such wavefields are classically used to trap microscopic particles in two dimensions (e.g., Ding et al. 2012, Tran et al. 2012). Depending on the properties of the particles (density, compressibility, and size) and of the surrounding medium, particles can be trapped either at the pressure nodes, antinodes, or midpoints situated along the nodal line at equal distance between two nodes (see, e.g., Silva et al. 2019). In any case, due to the multiplicity of trapping points and the absence of energy localization, a single particle cannot be moved independently from other neighboring particles. Thus, all particles present in the system are moved collectively with such wavefields.



energy) near the particle. A natural idea to achieve such localization is to use laterally or radially focalized waves (for 2D and 3D selective trapping, respectively). This solution, adopted in optics, is also valid in acoustics for particles attracted at the pressure antinodes of an acoustic standing wave field, such as particles less dense and more compressible than the surrounding liquid (see Equations 44 and 45). Nevertheless, particles more stiff and more dense than the surrounding liquid, such as solid particles, cells, and most droplets, migrate toward the pressure nodes of a standing wavefield (Gorkov 1962). Such particles would be expelled from the focus of a focalized wave, which precludes the use of focused waves to trap most particles of practical interest. For such particles, to ensure particle trapping it is necessary to concentrate the energy, but with a minimum at the wave focus surrounded by a ring of high intensity.

**4.1.1. Cylindrical vortices.** For 2D particle trapping, this apparently paradoxical problem can be solved by using some specific wavefields called cylindrical acoustical vortices (**Figure 3**). These wave structures are called acoustical vortices (similar to optics where they are called optical vortices) or helical acoustic waves owing to their helical wave front spinning around a phase singularity, whose phase structure resembles a hydrodynamic vortex. Nevertheless, since they are solutions of the wave equation, they do no carry any vorticity. This class of waves was originally introduced by Nye & Berry (1974) when they studied wave phase singularities and, in particular, so-called screw dislocations. The phase singularity on the central beam axis ensures a canceling of the amplitude on this axis, surrounded by a bright ring that can be used to trap particles laterally (Courtney 2014). In the field of acoustics, acoustical vortices were first introduced (and experimentally synthesized) by Hefner & Marston (1999). Mathematically, these wave structures can be simply introduced as a set of separated variable solutions in cylindrical coordinates, $\Psi(r, \theta, z) = f(r)g(\theta)h(z)$,

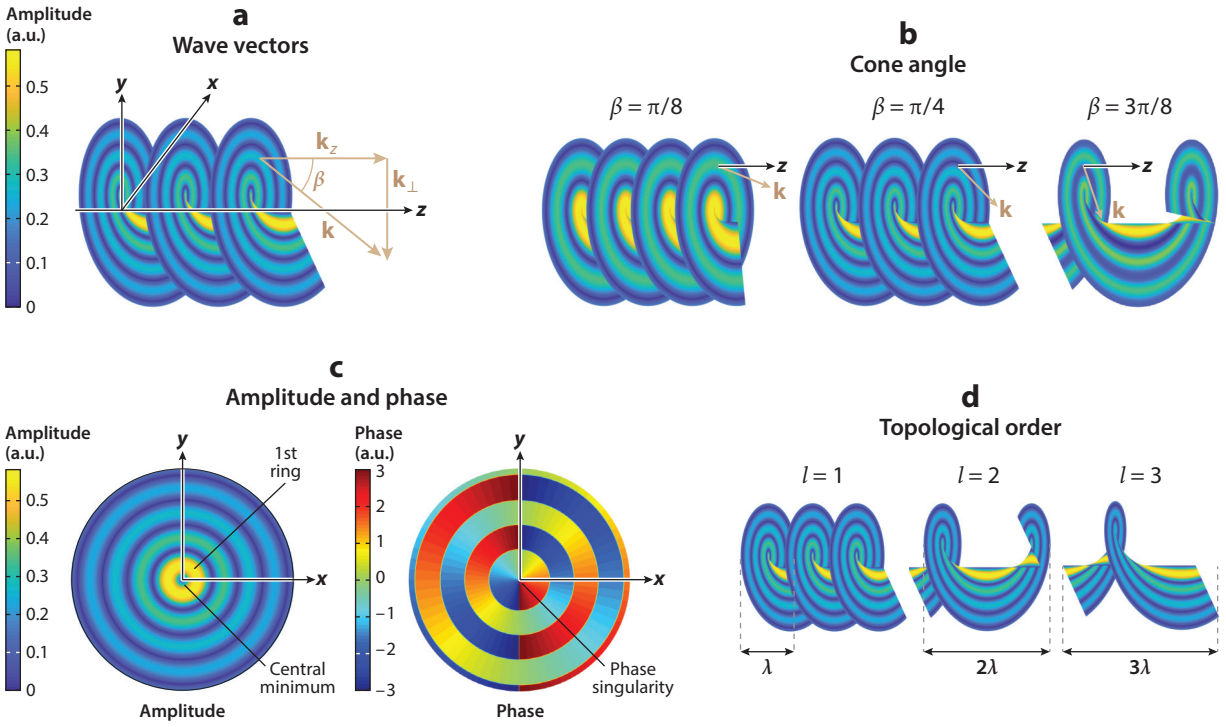


**Figure 3**

Bessel cylindrical vortices. (*a*) Equiphase surface of a Bessel cylindrical vortex (of topological order $l = 1$ and cone angle $\beta = \pi/4$). The color field corresponds to the pressure amplitude. The axial component $\mathbf{k}_z$, the lateral component $\mathbf{k}_\perp$, and the total wave vector $\mathbf{k} = \mathbf{k}_z + \mathbf{k}_\perp$ are shown. Note that $\mathbf{k}_\perp$ turns around the wave axis as the wave propagates along $z$-axis. (*b*) Equiphase surfaces of a cylindrical vortex (of topological order $l = 1$) for different cone angles $\beta = \arctan k_\perp/k_z$. As the cone angle increases, the lateral evolution of the vortex is more rapid while its axial evolution is slower. (*c*) Lateral evolution of the amplitude and phase. The amplitude vanishes at the $z$-axis, and this central minimum is surrounded by a ring of high intensity. Then the field is a succession of bright rings (high amplitude) of decreasing intensity and dark rings (low amplitude). Inside the first ring, the phase evolves from 0 to $2\pi$ when $\theta$ goes from 0 to $2\pi$, with a phase singularity at the center. Laterally the phase undergoes some phase jump of $\pi$ each time the sign of the Bessel function $J_l(kr)$ changes. (*d*) Equiphase surfaces of Bessel cylindrical vortices of different topological orders $l = 1, l = 2$, and $l = 3$.

of the wave equation in the Fourier space, i.e., the Helmholtz equation,

$$\Delta\Psi + k^2\Psi = 0 \Longleftrightarrow \frac{1}{r}\frac{\partial}{\partial r}\left(r\frac{\partial\Psi}{\partial r}\right) + \frac{1}{r^2}\frac{\partial^2\Psi}{\partial\theta^2} + \frac{\partial^2\Psi}{\partial z^2} + k^2\Psi = 0.$$

Indeed, an orthogonal set of solutions of this equation, which we term Bessel cylindrical vortices, is given by

$$\Psi(r,\theta,z,t) = A\,J_l(k_\perp r)\,\exp[i(l\theta + k_z z - \omega t)], \qquad 45.$$

where $A$ is the amplitude of the vortex, $J_l$ is the cylindrical Bessel function of the first kind of order $l$, $\mathbf{k}$ is the wave vector, $k = \|\mathbf{k}\| = \omega/c_0$ is the wave number, $c_0$ is the speed of sound, $l \in \mathbb{Z}$ is an integer called the topological charge, $k_z = \mathbf{k}\cdot\mathbf{z}$ is the projection of the wave vector over the propagation axis $\mathbf{z}$, and $k_\perp$ is defined as $\sqrt{k^2 - k_z^2}$ (see **Figure 3** for a visual representation of the different parameters). These beams are defined by three parameters: their angular frequency $\omega$, their topological order $l$, and the so-called cone angle $\beta = \arccos(k_z/k)$, which defines the angle

between the wave vector **k** and the propagation axis **z**. For $l = 0$, the field becomes invariant over $\theta$ and the lateral evolution is given by $J_0(kr)$, which exhibits a maximum at $r = 0$. Thus, this wavefield is not a vortex but simply a laterally focalized wave. Thus, vortices only refer to beams of topological order $|l| > 1$. These waves are propagative over $\theta$ and $z$ and stationary over $r$, with a lateral evolution given by the Bessel function. Bessel functions of order $|l| > 1$ all exhibit a minimum at $r = 0$ and then oscillate inside a decreasing envelope, evolving as $1/\sqrt{r}$.

These waves have good properties for lateral trapping of particles. Indeed, the canceling of the Bessel function $J_l(k_\perp r)$ of order $|l| > 1$ at $r = 0$ and then its increase up to a maximum creates a gradient trap that keeps the particle at the center.

Some asymptotic forms of these Bessel beams exist in the approximation of small conical angles ($\beta \ll 1$) between the wave number and the propagation axis, i.e., in the so-called paraxial approximation. The solutions of the paraxial approximation of the Helmholtz equation are the so-called Laguerre–Gaussian beams, which take the form

$$\Psi(r,\theta,z,t) = \frac{A}{w(z)}\left[\frac{\sqrt{2}r}{w(z)}\right]^{|l|} L_p^{|l|}\left[\frac{2r^2}{w(z)^2}\right]\exp\left\{\frac{-r^2}{w^2(z)} + i\left[l\theta + (2p+|l|+1)\arctan\left(\frac{z}{z_R}\right) - \frac{r^2 kz}{2(z^2+z_R^2)}\right]\right\},$$

where $L_p^{|l|}$ is the associated Laguerre polynomial, $w(z) = w_0\sqrt{1+z^2/z_R^2}$ is the beam width at position $z$ along the wave propagation axis, $w_0$ is the beam waist, $z_R = \pi w_0^2/\lambda$ is the Rayleigh range, $\lambda$ is the wavelength, and $(2p+l+1)\arctan(z/z_R)$ is the Gouy phase. These waves are common in optics since Gaussian beams are good approximations of the field produced by a laser. Their intensity is mostly localized close to the beam axis since their amplitude decreases exponentially as $\exp[-r^2/w^2(z)]$ with a radial extent equal to $w(z)$. Thus, these waves do not carry an infinite energy and can be synthesized experimentally (contrary to their Bessel counterpart).

Finally, if we push the approximation of Bessel beams to vanishing conical angles $\beta \to 0$, then we have $k_z \to k$ and $k_\perp \to 0$ and Bessel cylindrical vortices turn into so-called R-vortices,

$$\Psi = A\, r^J e^{i(l\theta + kz - \omega t)}.$$

It is interesting to note (as demonstrated by Fan & Zhang 2019) that at small cone angles, the axial component of the acoustic velocity can contribute significantly to the kinetic energy and hence to the radiation force. This can lead to a reverse behavior wherein particles denser and stiffer than the surrounding medium are trapped at the center of Bessel beams of topological order $m = 0$, that is, at the pressure maximum of laterally focalized waves.

Cylindrical vortices are interesting for lateral $(x,y)$ particle trapping. Nevertheless, as a consequence of their invariance in the $z$-direction, they can only push or pull the particles in this direction (Marston 2006, 2009; Baresch et al. 2013b; Fan & Zhang 2019; Gong et al. 2019).

**4.1.2. Spherical or focused vortices.** As first proposed by Baresch et al. (2013a), one way to obtain a 3D localized trap is to use the spherical analogs of cylindrical acoustical vortices, the so-called spherical vortices (also sometimes termed focused vortices) (**Figure 4*a***). Indeed, these wavefields focalize the energy in three dimensions, while maintaining a minimum at the focal point. These fields, like their cylindrical counterparts, are a set of orthogonal separate-variable

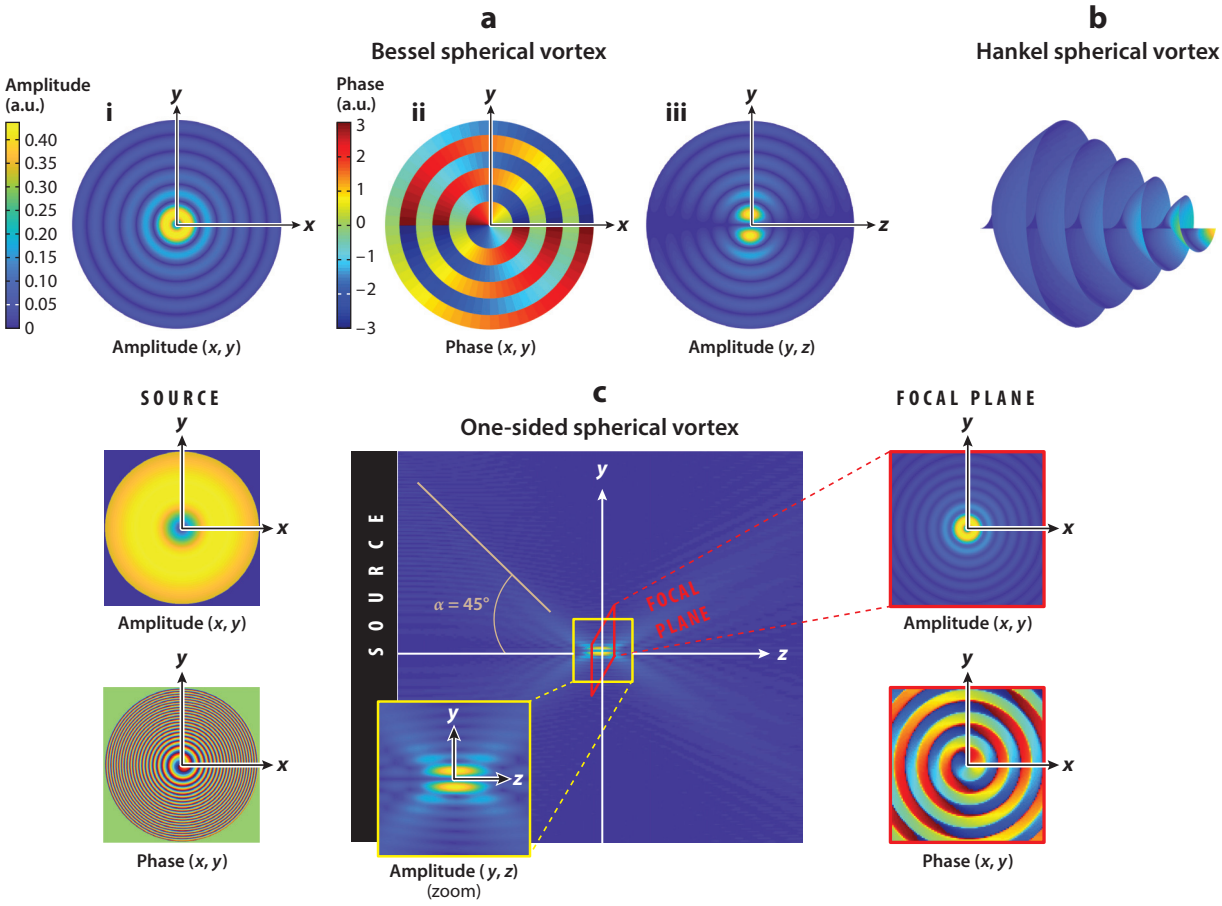


**Figure 4**

Spherical vortices of topological order $(l, m) = (1, 1)$. (*a*) Amplitude and phase of a Bessel spherical vortex, corresponding to Equation 46. (*b*) Isophase surface of a converging Hankel vortex. (*c*) Amplitude and phase of a one-sided spherical vortex; $\alpha$ corresponds to the aperture of the source. The amplitude in the $(y, z)$ plane shows the focalization of the vortex; the amplitude and phase in the (*lower left*) source plane $(x, y)$ and in the (*lower right*) focal plane are also shown.

solutions of the Helmholtz equation, but in spherical coordinates $(r, \theta, \varphi)$,

$$\Psi(r, \theta, \varphi) = A j_l(kr) P_l^m(\cos\theta) \exp\left[(i(m\varphi - \omega t)\right], \qquad 46.$$

where $j_l(kr)$ is the spherical Bessel function of the first kind of order $l \in \mathbb{Z}$, $P_l^m$ is the associated Legendre polynomial of order $(l, m)$, and $m$ is the topological charge, an integer satisfying $-l \leq m \leq l$. Similar to cylindrical vortices, the field is invariant over $\varphi$ for a topological charge $m = 0$, and thus the wavefield is no longer a vortex but simply a focalized wave. In particular, the case $(m, l) = (0, 0)$ corresponds to a spherically focused wave. Thus, we refer to spherical vortices as waves with topological order $|m| \geq 1$. These waves are stationary in $r$ and $\theta$ and propagative over $\varphi$. The central phase singularity is surrounded by a toroidal bright shell, which provides a good framework for 3D trapping (**Figure 4*a*, subpanel *i***). We can nevertheless note that the $z$-axis remains a specific axis around which the phase is spinning (**Figure 4*a*, subpanel *ii***). This specificity can also be seen in Equation 46, since $\theta$ is the angle with respect to the $z$-axis. Owing to

the phase singularity over this axis, the amplitude cancels all along the axis (**Figure 4*a***, **subpanel *iii***), leading to a weaker trap in this direction.

Spherical vortices carry a finite amount of energy, but their synthesis requires one to position transducers all around a closed surface surrounding the vortex center. Since this is not feasible in most practical situations, one idea is to synthesize a wave that is as close as possible to a spherical vortex, but with a finite aperture. In the following we call such wavefields one-sided spherical vortices (see **Figure 4*c***). Similar to how a plane standing wave $A\cos(kx)\exp(-i\omega t)$ can be decomposed into two counter-propagating progressive waves, $A/2\exp(ikx-\omega t)+A/2\exp(-ikx-\omega t)$, an important element needed to synthesize one-sided spherical vortices is the decomposition of a Bessel spherical vortex into Hankel converging and diverging spherical vortices,

$$Aj_l(kr)P_l^m(\cos\theta)\exp\left[(i(m\varphi-\omega t)\right]=\frac{A}{2}\left[h_l^{(1)}(kr)+h_l^{(2)}(kr)\right]P_l^m(\cos\theta)\exp\left[i(m\varphi-\omega t)\right],$$

where $h_l^{(1)}$ is the Hankel function of the first kind corresponding to the converging part and $h_l^{(2)}$ is the Hankel function of the second kind corresponding to the diverging part.

Thus a one-sided spherical vortex can be generated by synthesizing a section of a Hankel converging vortex (Baudoin et al. 2019) (see **Figure 4*b*** for a representation of the isophase surface of a Hankel vortex). This is possible with a system controlling the phase or the amplitude of a vibration on a given surface (which can be for example a portion of a sphere or a plane). **Figure 3*c*** gives an example of a one-sided spherical vortex synthesized from a control disk (wherein the amplitude and phase of the intersection of a Hankel spherical vortex with this disk is imposed). In this example, the aperture angle is 45° and the distance between the source and the focal plane is 20λ. This example shows that the interference between the converging Hankel vortex and the diverging Hankel vortex initiated at the passage through the focal point produces a standing gradient trap in the $z$-direction (see **Figure 4*c***, **subpanel *ii***). Nevertheless, since the signal is generated from only one side, the progressive part of the wave along the $z$-axis tends to push the particle away from the center in the direction of the wave propagation. This is this competition between the axial pushing force and the gradient restoring force, which makes the 3D trapping of particles particularly challenging. In addition, acoustic streaming can also contribute to push the particle away from the trap. In the field of acoustics, Baresch and coworkers were the first to demonstrate theoretically (Baresch et al. 2013a) and experimentally (Baresch et al. 2016) the ability of these beams to trap particles in three dimensions in the Mie regime. Interestingly, in the long-wavelength regime, Marzo et al. (2015) have shown through an optimization algorithm that acoustical vortices are optimal wavefields for 3D particle trapping for a given array of transducers with phase control. They have also demonstrated that two other types of wavefields, namely bottle traps and twin traps, are optimal for trapping in the direction of propagation and in one lateral direction, respectively.

## 4.2. Selective Particle Manipulation

In Section 2.3, we saw that the scattering coefficients were computed assuming axial symmetry. For a spherical particle, this assumption restricts the model to incident plane waves or spheres located at the focus of a spherical incident beam. Either a transversely polarized plane wave or acoustical vortices break the axial symmetry. Scattering of plane electromagnetic waves by a dielectric sphere has a known solution: the Lorenz–Mie theory. The Debye potentials are here particularly well suited for spherical particles. This case has also been studied for acoustic waves propagating in solids (Einspruch et al. 1960, Gaunard & Überall 1978), but the incident wave is always a plane wave, a case irrelevant for tweezers. To go further, researchers have developed two main methods

in optics. The first is to decompose the incident wave into plane waves and then use the previous results for each plane wave mode. The second method, called generalized Lorenz–Mie theory, looks for a decomposition of the arbitrary incident wave into a series of modes of the wave equation, generally the spherical basis (Maheu et al. 1987, Barton et al. 1988). This approach led to the first analytic results for radiation pressure exerted by an arbitrary beam on a dielectric sphere (Barton et al. 1989, Ren et al. 1994).

In acoustics, the growing interest in the manipulation of contactless particles has motivated research in this direction. The first method was used first, and the case of a particle located along the axis of propagation of an incident acoustic beam was modeled. Examples include axisymmetric beams (Marston 2006) or the more complex wave fronts of a helical Bessel beam (Marston 2008, 2009). The case of an arbitrary incident beam was addressed later (Sapozhnikov & Bailey 2013) and led to a complete expression of the radiation force.

The second strategy has also been adapted to acoustics and requires three steps. First, a separated variable solution of the Helmholtz equation in free space and in spherical coordinates is well known,

$$\phi(\mathbf{r},\omega) = \phi_a \sum_{n=0}^{\infty} \sum_{|m|<n} A_l^m P_l^m(\cos\theta) \exp(im\varphi) j_l(k_0 r). \qquad 47.$$

The series coefficients $A_l^m$ are called the beam shape coefficients. Using normalized spherical harmonics, defined by $Y_l^m = \sqrt{(2l+1)(l-m)!/4\pi(l+m)!}P_l^m(\cos\theta)\exp(im\varphi)$, leads to another equivalent set of beam shape coefficients, $\hat{A}_l^m$. The term $\phi_a$ is an optional factor used to obtain dimensionless beam shape coefficients. Previous theories (King 1934, Hasegawa et al. 2000) assumed azimuthal symmetry and hence $m = 0$. By assuming linear scattering and a spherical basis centered on the spherical scatterer, one can see that the beam shape coefficients of the scattered wave are proportional to the incident ones, $R_l^m A_l^m$. However, the boundary conditions, i.e., spherical divergence of the scattered wave, lead to the replacement of Bessel functions by Hankel functions of the first kind. As with Hasegawa et al. (2000), the integration of Equation 42 can then be performed on a fixed spherical surface located in the far field. This generalization was achieved independently by Silva (2011) and by Baresch et al. (2013b). At this stage, $A_l^m$ and $R_l^m$ are two sets of unknown coefficients, and identifying them is the last step required to compute the radiation force. The beam shape coefficients are defined by a scalar product of the field and the spherical harmonics. However, they are functions of the position of the sphere and hence their numerical evaluation in a 3D domain is time consuming and requires high precision. Different strategies exist to alleviate this problem (Gouesbet et al. 2010). An effective solution used in optics is to translate and rotate the spherical basis using the addition theorem to trace the sphere and obtain the new coefficients. This solution was adapted to acoustics by Baresch et al. (2013b). Lastly, to complete the generalization of Hasegawa & Yosioka (1969) to arbitrary incident beams, one must compute the scattering coefficients, $R_l^m$. This last step was also carried out by Baresch et al. (2013b). The axisymmetry and the resulting simplification made before are no longer valid (see Section 2.3). The acoustic displacement field inside the elastic particle can be decomposed into three scalar potentials, one for the longitudinal waves $\phi$ and two for the Debye potentials for shear waves $\psi$ and $\chi$, with $\mathbf{A}(r,\theta,\varphi) = \nabla\wedge\nabla\wedge(\mathbf{r}\psi) + \nabla\wedge(\mathbf{r}\chi)$. These potentials are solutions of the Helmholtz scalar equation and thus can be written as a series of spherical functions, as above. Compared to incident plane waves, the boundary conditions lead to a system of four linear equations relating the four potentials, one in the fluid and three in the elastic particle. This system is actually made up of one independent equation describing one of the shear elastic modes. Therefore, this mode cannot be excited by an incident longitudinal wave. The remaining system of three equations is

identical to the one obtained by Faran (1951). As a consequence, the azimuthal dependence can be dropped, $R_l^m = R_l$. The complete model of Baresch et al. (2013b) led to the first numerical study of the radiation pressure exerted by an arbitrary field on an elastic spherical particle. It used $A_l^m$ and, to facilitate comparison with Sapozhnikov & Bailey (2013) and Silva (2011), the radiation force expression is rewritten here with the $\hat{A}_l^m$ set,

$$F_x = -\frac{\langle \tilde{V} \rangle_a}{k_0^2} \sum_{n=0}^{\infty} \sum_{|m|<n} \Im \left( Q_n^{-m} \hat{A}_l^{m*} \hat{A}_{l+1}^{m-1} C_n + Q_n^m \hat{A}_l^m \hat{A}_{l+1}^{m+1*} C_n^* \right), \quad 48.$$

$$F_y = +\frac{\langle \tilde{V} \rangle_a}{k_0^2} \sum_{n=0}^{\infty} \sum_{|m|<n} \Re \left( Q_n^{-m} \hat{A}_l^{m*} \hat{A}_{l+1}^{m-1} C_n + Q_n^m \hat{A}_l^m \hat{A}_{l+1}^{m+1*} C_n^* \right), \quad 49.$$

$$F_z = -2\frac{\langle \tilde{V} \rangle_a}{k_0^2} \sum_{n=0}^{\infty} \sum_{|m|<n} \Im \left( T_n^m \hat{A}_l^{m*} \hat{A}_{l+1}^m C_n \right), \quad 50.$$

where $\langle \tilde{V} \rangle_a = k_0^2 \rho_0 |\phi_a|^2/4 = |p_a|^2/(4\rho_0 c_0^2)$ is a dimensional factor. It should be replaced by $1/(4\rho_0 c_0^2)$ if $\phi_a$ is not introduced in the spherical decomposition of the incident field (Equation 47). The terms $Q_n^m = \sqrt{(n+m+1)(n+m+2)}/\sqrt{(2n+1)(2n+3)}$ and $T_n^m = \sqrt{(n+m+1)(n-m+1)}/\sqrt{(2n+1)(2n+3)}$ are two coefficients related to the amplitude of the spherical harmonics. These two set of coefficients are identical in Baresch et al. (2013b) and Sapozhnikov & Bailey (2013). The ones obtained by Silva (2011) contain an error coming from the first step described above that required a reindexing of the series. The term $C_n = R_n^* + R_{n+1} + 2R_n^* R_{n+1}$ is the coefficient that makes explicit the dependence of the radiation force on the scattered waves, $R_n^* R_{n+1}$, or the cross product between incident and scattered waves, $R_n^* + R_{n+1}$. This coefficient can also be written with the S-matrix, $S_n = 1 + 2R_n$, so that we have $2C_n = S_n^* S_{n+1} - 1$. This relates the outgoing modes of order $n$ and $n+1$ (Sapozhnikov & Bailey 2013, Marston & Zhang 2017). Using equations 32 and 34 of Sapozhnikov & Bailey (2013), one can straightforwardly show that the two expressions of the radiation force are identical. This complete model gives a quantitative prediction of the radiation force. Some examples are given below for a bead of silica.

One specific feature of selective tweezers compared to standing wave traps is the selectivity. In the following text, $(r, \theta, z)$ refer to cylindrical coordinates, with $z$ corresponding to the principal axis of the one-sided spherical vortex. The radial selectivity of a one-sided spherical vortex at 50 MHz (corresponding to a wavelength of 30 μm) is shown in **Figure 5*a***. A negative force means that the bead is pulled toward the vortex axis. The trap has a radius of 0.42λ when the numerical aperture is 0.87, corresponding to a half angle of 60°. The radiation pressure scales in nano-Newtons for a moderate acoustic driving pressure of 1 MPa. This trapping force is relevant compared to forces in biological object manipulation and deformation. The azimuthal force is of similar amplitude (**Figure 5*b***). A bead initially located in the potential well will spiral around the vortex axis and in the end reach its equilibrium position at $r = 0$.

The axial selectivity and trap stiffness are also strongly dependent on the numerical aperture (**Figure 6*a***). The stiffness, selectivity, and force amplitude are weaker in the axial direction than in the lateral one since the beam is progressive on this axis. The force is positive (thus pushing the particle) when the bead is located before the focus. On the contrary, when the bead is downstream, the axial force is negative (thus pulling the bead toward the focus). This essential and specific feature of optical tweezers (Ashkin 2011) ensures trapping in the three dimensions. When the

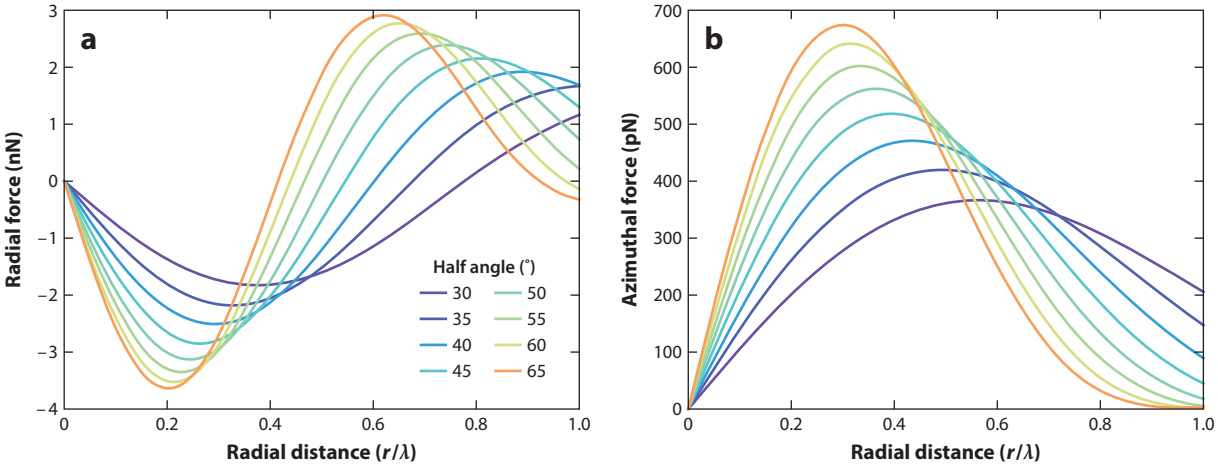


**Figure 5**

Radial (*a*) and azimuthal (*b*) forces of a one-sided spherical vortex on a sphere of silica; the wavelength λ is 30 μm. Forces are computed for a maximum pressure of 1 MPa at the focus and a sphere of radius 0.15λ. The trap stiffness and the selectivity increase with the numerical aperture.

radius of the bead is increased (**Figure 6*b***), the scattering force increases, and for a bead that is too large the axial trapping is lost.

3D trapping at the focus of a one-sided focused acoustical vortex was demonstrated numerically from these formulas (Baresch et al. 2013a) and then experimentally (Baresch 2014, Baresch et al. 2016). Here, the tweezers' pulling restoring force was high enough to compensate for the particle weight and the streaming drag force. A one-sided focused acoustical vortex was also able to push upward and levitate particles in air (Marzo et al. 2015).

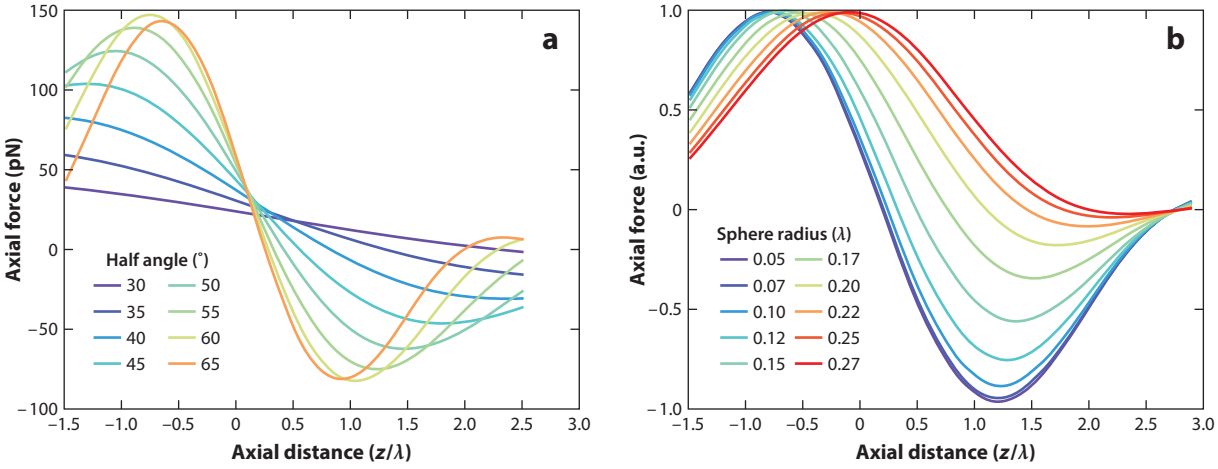


**Figure 6**

The axial force of a one-sided spherical vortex on a sphere of silica; the wavelength λ is 30 μm. (*a*) The trap stiffness increases with the numerical aperture. Forces are computed for a maximum pressure of 1 MPa at the focus and a sphere of radius 0.15λ. (*b*) The axial restoring force is lost for spheres that are too large.

### 4.3. Fluid Manipulation with Acoustical Vortices

Acoustical vortices carry pseudo-angular momentum. Thus, the nonlinear transfer of this pseudo-angular momentum to the fluid through wave attenuation results in a streaming flow whose topology is mainly controlled by the topology of the acoustic vortex. Anhäuser et al. (2012) provided the first estimation of this effect. Then, Riaud et al. (2014) resolved the complete problem by extending Eckart's theory to the case of Bessel cylindrical acoustical vortices. Starting from Eckart's vorticity diffusion equation in the steady case,

$$\Delta\bar{\boldsymbol{\Omega}} = -\frac{b}{\rho_0^2}\nabla\tilde{\rho}\times\nabla\frac{\partial\tilde{\rho}}{\partial t},$$

with $\bar{\boldsymbol{\Omega}} = \nabla\times\bar{\mathbf{v}}$ and $\tilde{\rho}$ given by Equation 45, they were able to compute the velocity field in the same configuration as Eckart, i.e., in an infinitely long cylinder of radius $r_0$ axially illuminated by a beam of finite radial extension, $r_1 < r_0$. They demonstrated that acoustical streaming in this configuration is the superposition of a poloidal flow (also predicted by Eckart in the case of a plane wave) and a toroidal flow that relies on the helical nature of the acoustical vortex. Interestingly, they showed that in some specific configurations, the direction of the poloidal flow can be reversed compared to the plane wave case, and the fluid can recirculate toward the center of the transducer (**Figure 7**). This can be explained by the existence of a shadow zone at the center of the beam wherein the fluid can recirculate.

Soon after, Hong et al. (2015) showed experimentally the toroidal flow predicted by this theory in an essentially 2D configuration. More recently, Baresch et al. (2018) evidenced the flow produced by a one-sided focused vortex and showed that the fluid is both pushed in the direction

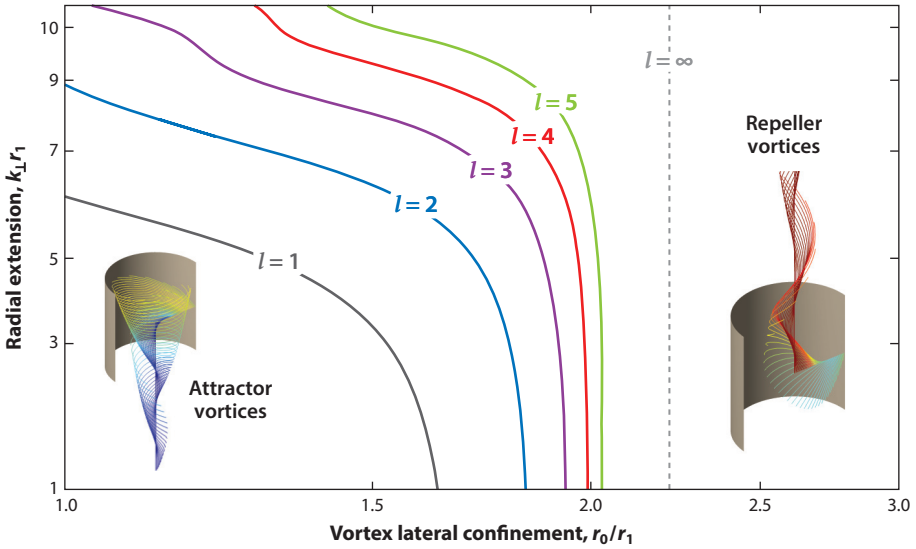


**Figure 7**

Flow structures induced by Bessel cylindrical vortices. The lines delimit the transition between attractor vortices, with a poloidal flow oriented toward the center of the source (located downward), and repeller vortices corresponding to the classic configuration, where the fluid is pushed away from the source. The ratio $r_0/r_1$ is the ratio between the radius of the cylinder and the lateral extension of the beam, $l$ is the topological charge of the vortex, and $k_\perp$ is the projection of the wave vector in a plane orthogonal to the beam axis. Figure adapted with permission from Riaud et al. (2014).

of the wave propagation and set in rotation around the propagation axis due to the helical nature of the wave. From a theoretical perspective, M. Baudoin et al. (submitted manuscript) calculated analytically the orbital acoustic streaming produced by a Bessel spherical vortex. As the resolution of this problem from Eckart's equation is intricate, they proposed another method based on Equation 29 and the use of Green's function of the Stokes equation. They showed that the resulting flow is purely orbital (since $\varphi$ is the only propagative component of a Bessel spherical vortex) with a confined flow structure located near the focal point.

## SUMMARY POINTS

1. The manipulation of particles and fluids with acoustic waves is enabled by two nonlinear effects: acoustic radiation pressure and acoustic streaming, respectively.
2. Since both acoustic and optical radiation pressure are proportional to the wave intensity divided by the sound speed, acoustic tweezers enable the application of forces several orders of magnitude larger than their optical counterpart at the same wave intensity.
3. Acoustic tweezers relying on plane standing waves can trap and move particles collectively, but the multiplicity of nodes and antinodes does not allow one to move one particle independently of other neighboring particles, i.e., to trap particles selectively.
4. To achieve selectivity, we need to localize the acoustic energy. Since many particles of interest are trapped at acoustic wave pressure nodes, focused waves cannot be used in this case. Localized traps for this type of particles can be achieved with some specific wave structures called acoustical vortices, which allow one to both focalize the acoustic energy and obtain a pressure minimum at the focal point surrounded by a bright ring, which serves as a trap.
5. To achieve 3D selective trapping with one-sided tweezers, it is necessary to generate a wave structure that compensates for the particles' tendency to be pushed in the wave direction. This task can be be achieved with one-sided spherical vortices.
6. Acoustical vortices can generate some localized flow structures, whose topology relies on the topology of the acoustical vortex.

## FUTURE ISSUES

1. Particles assembly: The 3D selective manipulation of particles with acoustic tweezers has recently been demonstrated. It is essential in the future to demonstrate that it is not only possible to capture particles individually but also to assemble them to form clusters of precisely assembled objects.
2. Force calibration: For applications, it would also be necessary to calibrate the force applied by the tweezers as a function of the input power. Indeed, this calibration of the force would lead (as in optics but with forces several orders or magnitude larger) to many applications (e.g., the study of cells' mechanotransduction, the resistance of bio-objects to mechanical solicitations).
3. Further miniaturization: A significant step has recently been achieved in the miniaturization of acoustic tweezers. Nevertheless, acoustic coherent sources exist up to gigahertz, paving the way toward micrometric and even submicrometric particles manipulation.

The manipulation at this scale is both a technical and scientific challenge, since it is necessary to understand how acoustic radiation pressure and acoustic streaming will evolve at these scales.

4. Harmless selective manipulation of biological objects: It is also necessary to demonstrate that acoustical traps with large trapping force can be obtained at micrometric scales with harmless acoustic signals for biological objects. This is critical for all applications involving cells and microorganisms.
5. Measurement of acoustic streaming induced by acoustical vortices: Quantitative comparisons between experimentally synthesized velocity fields and theoretical developments are still lacking.



## DISCLOSURE STATEMENT

The authors are not aware of any biases that might be perceived as affecting the objectivity of this review.

## ACKNOWLEDGMENTS

The authors would like to express their gratitude to the colleagues and students who, over the years, shared their views with us and made this review possible, in particular D. Baresch, O. Bou Matar, J.-C. Gerbedoen, R. Marchiano, and A. Riaud.

## LITERATURE CITED

Allen CH, Rudnick I. 1947. A powerful high frequency siren. *J. Acoust. Soc. Am.* 19:857–65

Altberg W. 1903. Ueber die Druckkräfte der Schallwellen und die absolute Messung der Schallintensitt. *Ann. Phys.* 316:405–20

Anhäuser A, Wunenburger R, Brasselet E. 2012. Acoustical rotational manipulation using orbital angular momentum transfer. *Phys. Rev. Lett.* 109:034301

Apfel RE. 1981. Acoustic levitation for studying liquids and biological materials. *J. Acoust. Soc. Am.* 70:636–39

Ashkin A, Dziedzic JM, Bjorkholm JE, Chu S. 1986. Observation of a single-beam gradient force optical trap for dielectric particles. *Opt. Lett.* 11:288–90

Ashkin A. 2011. How it all began. *Nat. Photon.* 5:316–17

Baasch T, Dual J. 2018. Acoustofluidic particle dynamics: beyond the Rayleigh limit. *J. Acoust. Soc. Am.* 143:509–19

Baird MHI. 1963. Resonant bubbles in a vertically vibrating liquid column. *Can. J. Chem. Eng.* 41:52–55

Baker NV. 1972. Segregation and sedimentation of red blood cells in ultrasonic standing waves. *Nature* 239:398–99

Baresch D. 2014. *Pince acoustique: piégeage et manipulation d'un objet par pression de radiation d'une onde progressive*. PhD Thesis, Univ. Pierre Marie Curie, Paris, Fr. **https://tel.archives-ouvertes.fr/tel-01165034**

Baresch D, Thomas J-L, Marchiano R. 2013a. Spherical vortex beams of high radial degree for enhanced single-beam tweezers. *J. Appl. Phys.* 113:184901

Baresch D, Thomas J-L, Marchiano R. 2013b. Three-dimensional acoustic radiation force on an arbitrarily located elastic sphere. *J. Acoust. Soc. Am.* 133:25–36

Baresch D, Thomas J-L, Marchiano R. 2016. Observation of a single-beam gradient force acoustical trap for elastic particles: acoustical tweezers. *Phys. Rev. Lett.* 116:024301

Baresch D, Thomas J-L, Marchiano R. 2018. Orbital angular momentum transfer to stably trapped elastic particles in acoustical vortex beams. *Phys. Rev. Lett.* 121:074301

Barton JP, Alexander DR, Schaub SA. 1988. Internal and near-surface electromagnetic fields for a spherical particle irradiated by a focused laser beam. *J. Appl. Phys.* 4:1632–39
Barton JP, Alexander DR, Schaub SA. 1989. Theoretical determination of net radiation force and torque for a spherical particle illuminated by a focused laser beam. *J. Appl. Phys.* 66:4594–602
Baudoin M, Gerbedoen J-C, Riaud A, Bou Matar O, Smagin N, Thomas J-L. 2019. Folding a focalized acoustical vortex on a flat holographic transducer: miniaturized selective acoustical tweezers. *Sci. Adv.* 5:eaav1967
Beissner K. 1998. The acoustic radiation force in lossless fluids in Eulerian and Lagrangian coordinates. *J. Acoust. Soc. Am.* 103:2321–32
Biquard P. 1932a. Les ondes ultra-sonores. *Rev. d'Acoust.* 1:93–109
Biquard P. 1932b. Les ondes ultra-sonores II. *Rev. d'Acoust.* 1:315–55
Bjerknes VFJ. 1906. *Fields of Force*. New York: Columbia Univ. Press
Bopp VF. 1940. Energetische Betrachtungen zum Schaallstrahlungsdruck. *Ann. Phys.* 38:495–500
Borgnis FE. 1953. Acoustic radiation pressure of plane compressional waves. *Rev. Mod. Phys.* 25:653–63
Brillouin L. 1925. Sur les tensions de radiation. *Ann. Phys. X* 4:528–86
Brillouin L. 1936. Les pressions et tensions de radiation. *Rev. d'Acoust.* 5:99–111
Brillouin L. 1938. *Tensors in Mechanics and Elasticity*. New York: Academic
Brillouin L. 1956. Les tensions de radiation; leur interprétation en mécanique classique et en relativité. *J. Phys. Radium* 6:337–53
Buchanan RH, Jameson G, Oedjoe D. 1962. Cyclic migration of bubbles in vertically vibrating columns. *Ind. Eng. Chem. Fundam.* 1:82–86
Chen X, Apfel RE. 1996. Radiation force on a spherical object in the field of a focused cylindrical transducer. *J. Acoust. Soc. Am.* 101:2443–47
Coakley WT, Bardsley DW, Grundy MA, Zamani F, Clarke DJ. 1989. Cell manipulation in ultrasonic standing wave fields. *J. Chem. Tech. Biotechnol.* 44:43–62
Collins DJ, Morahan B, Garcia-Bustos J, Doerig C, Pleansku M, Neild A. 2015. Two-dimensional single-cell patterning with one cell per well driven by surface acoustic waves. *Nat. Commun.* 6:8686
Coulouvrat F. 1992. On the equations of nonlinear acoustics. *J. Acoust.* 5:321–59
Courtney CRP, Demore CEM, Wu H, Grinenko A, Wilcox PD, et al. 2014. Independent trapping and manipulation of microparticles using dexterous acoustic tweezers. *Appl. Phys. Lett.* 104:154103
Ding X, Li P, Lin S-C, Kirali B, Yue H, et al. 2012. On-chip manipulation of single microparticles, cells, and organisms using surface acoustic waves. *PNAS* 109:11105–9
Ding X, Li P, Lin S-C, Stratton ZS, Nama N, et al. 2013. Surface acoustic wave microfluidics. *Lab Chip* 13:3626–49
Dvorak V. 1874. Ueber die Entstehungsweise der Kundt'schen Staubfiguren. *Ann. Phys.* 227:634–39
Eckart C. 1948. Vortices and streams caused by sound waves. *Phys. Rev.* 73:68–76
Einspruch NG, Witterholt EJ, Truell R. 1960. Scattering of a plane transverse wave by a spherical obstacle in an elastic medium. *J. Appl. Phys.* 31:806–18
Eller A. 1968. Force on a bubble in a standing acoustic wave. *J. Acoust. Soc. Am.* 43:170–71
Embleton TFW. 1954. Mean force on a sphere in a spherical sound field. I. (Theoretical). *J. Acoust. Soc. Am.* 26:40–45
Fan X-D, Zhang L. 2019. Trapping force of acoustical bessel beams on a sphere and stable tractor beams. *Phys. Rev. Appl.* 11:014055
Faraday M. 1831. On a peculiar class of acoustical figures; and on certain forms assumed by groups of particles upon vibrating elastic surfaces. *Phil. Trans. R. Soc. Lond.* 121:299–340
Faran JJ. 1951. Sound scattering by solid cylinders and spheres. *J. Acoust. Soc. Am.* 23:405–18
Gaunard GC, Überall H. 1978. Theory of resonant scattering from spherical cavities in elastic and viscoelastic media. *J. Acoust. Soc. Am.* 63:1699–712
Glynne-Jones P, Mishra PP, Boltryk RJ, Hill M. 2013. Efficient finite element modeling of radiation forces on elastic particles of arbitrary size and geometry. *J. Acoust. Soc. Am.* 133:1885–93
Gong Z, Marston PL, Li W. 2019. *T*-matrix evaluation of three-dimensional acoustic radiation forces on nonspherical objects in Bessel beams with arbitrary order and location. *Phys. Rev. E* 99:063004

Gor'kov LP. 1962. On the forces acting on a small particle in an acoustic field in an ideal fluid. *Sov. Phys. Dokl.* 6:773–75

Gouesbet G, Lock JA, Gréhan G. 2010. Generalized Lorenz–Mie theories and description of electromagnetic arbitrary shaped beams: localized approximations and localized beam models, a review. *J. Quant. Spect. Rad. Transf.* 112:1–27

Gould RK. 1968. Simple method for calibrating small omnidirectional hydrophones. *J. Acoust. Soc. Am.* 43:1185–87

Gusev VE, Rudenko OV. 1979. Nonsteady quasi-one-dimensional acoustic streaming in unbounded volumes with hydrodynamic nonlinearity. *Sov. Phys. Acoust.* 25:493–97

Habibi R, Devendra C, Neild A. 2017. Trapping and patterning of large particles and cells in a 1D ultrasonic standing wave. *Lab Chip* 17:3279–90

Hagsäter SM, Gladsam Jensen T, Bruus H, Kutter JP. 2007. Acoustic resonances in microfluidic chips: full-image micro-PIV experiments and numerical simulations. *Lab Chip* 7:1336–44

Hasegawa T. 1977. Comparison of two solutions for acoustic radiation pressure on a sphere. *J. Acoust. Soc. Am.* 61:1445–48

Hasegawa T. 1979. Acoustic radiation force on a sphere in a quasi-stationary wave field—theory. *J. Acoust. Soc. Am.* 65:32–40

Hasegawa T, Kido T, Iizuka T, Matsuoka C. 2000. A general theory of Rayleigh and Langevin radiation pressures. *J. Acoust. Soc. Jpn.* 21:145–52

Hasegawa T, Ochi M, Matsuzawa K. 1981. Acoustic radiation force on a solid elastic sphere in a spherical wave field. *J. Acoust. Soc. Am.* 69:937–42

Hasegawa T, Yosioka K. 1969. Acoustic radiation force on a solid elastic sphere. *J. Acoust. Soc. Am.* 46:1139–43

Hefner BT, Marston PL. 1999. An acoustical helicoidal wave transducer with applications for the alignment of ultrasonic and underwater systems. *J. Acoust. Soc. Am.* 106:3313–16

Herrey EM. 1955. Experimental studies on acoustic radiation pressure. *J. Acoust. Soc. Am.* 27:891–96

Hertz G, Mende H. 1939. Der Schallstrahlungsdruk in Flussigkeiten. *Z. Phys.* 114:354–67

Hong Z, Zhang J, Drinkwater B. 2015. Observation of orbital angular momentum transfer from Bessel-shaped acoustic vortices to diphasic liquid-microparticle mixtures. *Phys. Rev. Lett.* 114:214301

Jackson JD. 1962. *Classical Electrodynamics*. New York: Wiley

Jiang X, Li Y, Liang B, Cheng J-C, Zhang L. 2016. Convert acoustic resonances to orbital angular momentum. *Phys. Rev. Lett.* 117:034301

Jiménez N, Picó R, Romero-García V, García-Raffi LM, Cemrana F, Staliunas K. 2018. Sharp acoustic vortex focusing by Fresnel-spiral zone plates. *Appl. Phys. Lett.* 112:204101

Jiménez N, Picó R, Sánchez-Morcillo V, Romero-García V, García-Raffi LM, Staliunas K. 2016. Formation of high-order acoustic Bessel beams by spiral diffraction gratings. *Phys. Rev. E* 94:053004

Kamakura T, Sudo T, Matsuda K, Kumamoto Y. 1996. Time evolution of acoustic streaming from a planar ultrasound source. *J. Acoust. Soc. Am.* 100:132–38

Karlsen JT, Augustsson P, Bruus H. 2016. Acoustic force density acting on inhomogeneous fluids in acoustic fields. *Phys. Rev. Lett.* 117:114504

Karlsen JT, Bruus H. 2015. Forces acting on a small particle in an acoustical field in a thermoviscous fluid. *Phys. Rev. E* 92:043010

King L. 1934. On the acoustic radiation pressure on spheres. *Proc. R. Soc. Lond. A* 147:212–40

Klein E. 1938. Absolute sound intensity in liquids by spherical torsion pendula. *J. Acoust. Soc. Am.* 9:312–20

Kuznetsov VP. 1970. Equations of nonlinear acoustics. *Sov. Phys. Acoust.* 16:467–70

Lenshof A, Laurell T. 2010. Continuous separation of cells and particles in microfluidic systems. *Chem. Soc. Rev.* 39:1203–17

Li Y, Jiang X, Liang B, Cheng J-C, Zhang L. 2015. Metascreen-based acoustic passive phased array. *Phys. Rev. Appl.* 4:024003

Liberman LN. 1949. The second viscosity of liquids. *Phys. Rev.* 75:1415–22

Lighthill J. 1978. Acoustic streaming. *J. Sound Vib.* 61:391–418

Maheu B, Gouesbet G, Gréhan G. 1987. A concise presentation of the generalized Lorenz-Mie theory for arbitrary location of the scatterer in an arbitrary incident profile. *J. Opt.* 19:59–67

Marston PL. 2006. Axial radiation force of a Bessel beam on a sphere and direction reversal of the force. *J. Acoust. Soc. Am.* 120:3518
Marston PL. 2008. Scattering of a Bessel beam by a sphere: II. Helicoidal case and spherical shell example. *J. Acoust. Soc. Am.* 124:2905–10
Marston PL. 2009. Radiation force of a helicoidal Bessel beam on a sphere. *J. Acoust. Soc. Am.* 120:3539–47
Marston PL, Zhang L. 2017. Relationship of scattering phase shifts to special radiation force conditions for spheres in axisymmetric wave-fields. *J. Acoust. Soc. Am.* 141:3042–49
Marzo A, Seah SA, Drinkwater BW, Sahoo DR, Long B, Subramanian S. 2015. Holographic acoustic elements for manipulation of levitated objects. *Nat. Commun.* 6:8661
McIntyre ME. 1981. On the "wave momentum" myth. *J. Fluid Mech.* 106:331–47
Moudjed B, Botton V, Henry D, Ben Hadid H, Garandet J-P. 2014. Scaling and dimensional analysis of acoustic streaming jets. *Phys. Fluids* 26:093602
Neuman KC, Nagy A. 2008. Single-molecule force spectroscopy: optical tweezers, magnetic tweezers and atomic force microscopy. *Nat. Meth.* 5:491–505
Nyborg WL. 1953. Acoustic streaming due to attenuated plane waves. *J. Acoust. Soc. Am.* 25:68–75
Nye JF, Berry MV. 1974. Dislocations in wave trains. *Proc. R. Soc. Lond. A* 336:164–90
Ozcelik A, Rufo J, Guo F, Gu Y, Li P, et al. 2018. Acoustic tweezers for the life sciences. *Nat. Meth.* 15:1021–28
Peierls R. 1985. Momentum and pseudomomentum of light and sound. In *Highlights of Condensed Matter Theory*, ed. F Bassani, F Fumi, MP Tosi, pp. 237–55. Bologna, Italy: Soc. Ital. Fisica
Post EJ. 1953. Radiation pressure and dispersion. *J. Acoust. Soc. Am.* 25:55–60
Post EJ. 1960. Meaning and interpretation of acoustic momentum and acoustic radiation. *Phys. Rev.* 118:1113–17
Rayleigh L. 1884. On the circulation of air observed in Kundt's tubes, and some allied acoustical problems. *Philos. Trans. R. Soc. Lond.* 175:1–21
Rayleigh L. 1902. On the pressure of vibration. *Philos. Mag.* 3:338–46
Rayleigh L. 1905. On the momentum and pressure of gaseous vibrations, and on the connection with the virial theorem. *Philos. Mag.* 10:364–74
Ren KF, Gréhan G, Gouesbet G. 1994. Radiation pressure forces exerted on a particle arbitrarily located in a Gaussian beam by using the generalized Lorenz-Mie theory, and associated resonance effects. *Opt. Commun.* 108:343–54
Riaud A, Baudoin M, Thomas J-L, Bou Matar O. 2014. Cyclones and attractive streaming generated by acoustical vortices. *Phys. Rev. E* 90:013008
Riaud A, Baudoin M, Bou Matar O, Becera L, Thomas J-L. 2017a. Selective manipulation of microscopic particles with precursor swirling Rayleigh waves. *Phys. Rev. Appl.* 7:024007
Riaud A, Baudoin M, Bou Matar O, Thomas J-L, Brunet P. 2017b. On the influence of viscosity and caustics on acoustic streaming in sessile droplets: an experimental and a numerical study with a cost-effective method. *J. Fluid Mech.* 821:384–420
Richter VG. 1940. Zur Frage des Schallstrahlungsdruckes. *G. Z. Phys.* 115:97–108
Riley N. 2001. Steady streaming. *Annu. Rev. Fluid Mech.* 33:43–65
Romanenko EV. 1960. Experimental study of acoustic streaming in water. *Sov. Phys. Acoust.* 6:87–91
Rooney JA. 1973. Determination of acoustic power outputs in the microwatt-milliwatt range. *Ultrasound Med. Biol.* 1:13–16
Rudenko OV, Soluyan SI. 1971. Theory of non-stationary acoustic streaming. *Sov. Phys. Acoust.* 17:97–101
Rudnick I. 1977. Measurements of the acoustic radiation pressure on a sphere in a standing wave field. *J. Acoust. Soc. Am.* 62:20–22
Sapozhnikov OA, Bailey MR. 2013. Radiation force of an arbitrary acoustic beam on an elastic sphere in a fluid. *J. Acoust. Soc. Am.* 133:661–76
Schram CJ. 1984. *Separation of particles in liquid medium—using varied ultrasonic standing wave*. Eur. Patent 167406
Schwartz T, Petit-Pierre G, Dual J. 2013. Rotation of non-spherical micro-particles by amplitude modulation of superimposed orthogonal ultrasonic modes. *J. Acoust. Soc. Am.* 133:1260–68

Settnes M, Bruus H. 2012. Forces acting on a small particle in an acoustical field in a viscous fluid. *Phys. Rev. E* 85:016327

Silva GT. 2011. An expression for the radiation force exerted by an acoustic beam with arbitrary wavefront. *J. Acoust. Soc. Am.* 130:3541–44

Silva GT, Lopes JG, Leao-Neto JP, Nichols K, Drinkwater B. 2019. Particle patterning by ultrasonic standing waves in a rectangular cavity. *Phys. Rev. Appl.* 11:054044

Sölner K, Bondy C. 1936. The mechanism of coagulation by ultrasonic waves. *Trans. Faraday Soc.* 32:616–23

Stanikov YG. 1967. Streaming induced by finite amplitude sound. *Sov. Phys. Acoust.* 23:247–85

Svoboda K, Block SM. 1994. Biological applications of optical forces. *Annu. Rev. Biophys. Biomol. Struct.* 23:247–85

Thomas J-L, Marchiano R, Baresch D. 2017. Acoustical and optical radiation pressure and the development of single beam acoustical tweezers. *J. Quant. Spect. Rad. Transf.* 195:55–65

Tran SBQ, Marmottant P, Thibault P. 2012. Fast acoustic tweezers for the two-dimensional manipulation of individual particles in microfluidic channels. *Appl. Phys. Lett.* 101:114103

Whitworth G, Grundy MA, Coakley WT. 1991. Transport and harvesting particles using modulated ultrasound. *Ultrasonics* 29:439–44

Xie WJ, Wei B. 2002. Dependence of acoustic levitation capabilities on geometric parameters. *Phys. Rev. E* 66:026605

Yeo LY, Friend JR. 2014. Surface acoustic wave microfluidics. *Annu. Rev. Fluid Mech.* 46:379–406

Yosioka K, Kawasima Y. 1955. Acoustic radiation pressure on a compressible sphere. *Acustica* 5:167–73

Westervelt PJ. 1953. The theory of steady rotational flow generated by a sound field. *J. Acoust. Soc. Am.* 25:60–67

Wu JR. 1991. Acoustical tweezers. *J. Acoust. Soc. Am.* 89:2140–43

Annual Review of
Fluid Mechanics

Volume 52, 2020

# Contents

**Indexes**



**Errata**

An online log of corrections to *Annual Review of Fluid Mechanics* articles may be found at http://www.annualreviews.org/errata/fluid